Factors controlling variation of number-size distribution of submicron aerosol particles observed at Mt. Norikura

(乗鞍岳で観測されたサブミクロンエアロゾル粒子の個数粒径分布の変化の要因)

Chiharu NISHITA

(西田　千春)

A dissertation for the degree of Doctor of Science
Department of Earth and Environmental Sciences,
Graduate School of Environmental Studies, Nagoya University
(名古屋大学大学院環境学研究科　学位論文　博士　(理学))

2008

要旨

大気エアロゾル粒子の個数粒径分布は、大気エアロゾルを記述する重要な要素であり、大気放射に対するエアロゾルの影響を見積もるためにも不可欠な測定項目である。大気エアロゾル粒子のなかでも、直径約 100 nm 以下の粒子は、大気の放射収支にほとんど影響しない。しかし、大気放射に直接関与する直径約 100 nm 以上のエアロゾル粒子の個数粒径分布の変化を予測するためには、直径数 nm から 100 nm の粒径のエアロゾル粒子の、大気中における生成・成長・消滅の過程を理解することが必要である。しかし、これらの過程について十分な理解は得られていない。例えば、降水によるエアロゾル粒子の除去過程については、モデル計算や室内実験によって定量的な研究が行なわれているが、大気観測によってそれらの研究結果を確認した例は少ない。また、均一核生成とそれに続く粒子成長によって直径数ナノメートルのエアロゾル粒子が生成される過程 (新粒子生成) については、その過程の複雑さや測定技術の限界などにより、解明されていない点が多い。1990 年代以降、測定技術の進歩により、大気中の様々な場所で、直径 100 nm 以下の粒径範囲を含むエアロゾル粒子の個数粒径分布の観測が行なわれている。しかし、これまで、東アジア・西太平洋域上空の自由対流圏において観測を行なった例は少ない。

本研究は、東アジア・西太平洋域上空の自由対流圏におけるサブミクロンエアロゾル粒子の個数粒径分布と、その時間変化の要因を明らかにすることを目的とし、2001 年 9 月と 2002 年 8–9 月(全観測日数 48 日)に、飛騨山脈・乗鞍岳山頂近く (標高 2770 m) において、直径 9–300 nm のエアロゾル粒子の個数粒径分布の時系列観測を行なった。乗鞍岳で観測される自由対流圏のエアロゾルは、エアロゾル粒子やその前駆気体について観測地近くの発生源の影響をほとんど受けないため、降水による除去過程の影響を調べるのに適している。そこで、本研究では、乗鞍岳における観測結果から、降水によるエアロゾル粒子の除去係数を見積ることを試みた。一方、乗鞍岳山頂付近では、日中に吹く斜面上昇風 (谷風) により、自由対流圏のエアロゾルだけではなく、境界層に由来するエアロゾルも観測される。自由対流圏のエアロゾルと境界層のエアロゾルとでは、新粒子生成に関係する種々の要因が異なると予想される。そこで、本研究は、この両者の比較から、大気中における新粒子生成に関する新たな知見の獲得を試みた。

気塊の後方流跡線上の客観解析データより、過去 24 時間に気塊が経験した降水量(蓄積降水量)を見積もり、見積もられた蓄積降水量と乗鞍岳で観測された自由対流圏のエアロゾル粒子の個数粒径分布との関係を調べた。蓄積降水量が 0 mm から 20 mm に増加すると、直径 9 nm から 100 nm の粒子の総粒子数濃度は約半分に減少し、直径 100 nm から 300 nm の粒子の総粒子数濃度は約一桁減少するような関係が見られた。これらの結果から、乗鞍岳の自由対流圏のエアロゾル粒子の個数粒径分布の変化の要因として、蓄積降水量が重要であることが示された。さらに、蓄積降水量と粒子数濃度から、エアロゾル粒子の除去係数を見積もり、モデル計算による先行研究の結果と比較した。観測結果から見積もられた除去係数は、雲底下で雨滴と衝突すること (雲底下洗浄)

による除去係数よりも約二桁高かった。しかし、雲内で雲核として作用することを経て雨滴と衝突すること(雲内洗浄) による除去係数とは、ほぼ一致していた。これらのことから、エアロゾル粒子を除去する過程として、雲内洗浄が重要であると考えられる。

気塊の後方流跡線にもとづいて、観測された気塊を太平洋から輸送された気塊とアジア大陸から輸送されてきた気塊に分類し、これらの気塊で観測された自由対流圏のエアロゾル粒子の個数粒径分布を比較した。降水の影響の少ない場合には、太平洋上空から輸送された気塊中の蓄積モード粒子 (モード直径、約 100 nm) の個数濃度は、アジア大陸上空から輸送された気塊中の蓄積モード粒子の個数濃度とほとんど同じだった (中央値で約 400 cm^{-3})。しかし、エイトケンモード粒子 (モード直径、約 50 nm) の個数濃度は、アジア大陸上空から輸送された気塊 (中央値で約 230 cm^{-3}) よりも、太平洋上空から輸送された気塊 (中央値で約 890 cm^{-3}) で高かった。このことから、乗鞍岳の自由対流圏エアロゾル中のエイトケンモード粒子の個数濃度の変化の要因として、気塊の輸送経路が重要であることがわかった。

エアロゾル粒子の個数粒径分布に核生成モード (直径 20 nm に現れる峰) が観測された日 (ここではイベント日と呼ぶ) は、晴天日 23 日のうち 4 日あった。核生成モードの出現は、その気塊で数時間から半日以内に新粒子生成が起きたことを示す。核生成モード粒子は、自由対流圏のエアロゾル中では観測されず、谷風によって境界層より観測地へ輸送されたエアロゾル中でのみ観測された。観測された核生成モード粒子は、境界層内で生成され、谷風によって観測地へ輸送されたものと考えられる。

新粒子生成に関する要因について検討するために、イベント日と非イベント日の谷風条件時に観測された SO_2 や NH_3、既存粒子の濃度の比較を行なった。H_2SO_4 や NH_3 が、新粒子生成の前駆気体として重要であるならば、SO_2 や NH_3 の濃度が高いほど新粒子生成に有利であると考えられる。しかし、非イベント日に比べてイベント日の SO_2 や NH_3 の濃度は低かった (平均で、非イベント日の約半分)。一方、既存粒子は、新粒子生成に寄与する低揮発性気体成分や、生成されたばかりの粒子のシンクとして働くため、既存粒子の濃度が低いほど新粒子生成に有利であると考えられる。観測結果によれば、非イベント日に比べてイベント日の既存粒子の濃度は低かった (平均で、非イベント日の約半分)。このことから、乗鞍岳において核生成モード粒子が観測されるための条件として、境界層で既存粒子濃度が低いことが重要であると考えられる。

本研究は、乗鞍岳山頂付近で大気観測を行なうことにより、これまで観測例の少なかった東アジア・西太平洋域上空の自由対流圏におけるサブミクロンエアロゾル粒子の個数粒径分布、および、その変化の要因について明らかにした。本研究で得られた知見を総合することにより、大気中におけるエアロゾル粒子の個数粒径分布の変化について、エアロゾル粒子の生成・成長・除去過程を介した循環様式を提示し、降水による除去過程が、エアロゾル粒子の個数粒径分布の循環を駆動する重要な過程であることを示唆した。

Contents

Abstract

Particle number-size distribution is an important element describing atmospheric aerosol and a crucial topic to evaluate aerosol effects on the Earth's radiation balance. Although aerosol particles with sizes smaller than about 100-nm diameter are less effective for radiative forcing, the knowledge of formation, growth and removal processes of aerosol particles from nanometer sizes upward is important to predict temporal evolution of number-size distribution of atmospheric aerosol particles. Wet deposition is the dominant removal process especially for submicron aerosol particles. Scavenging coefficient of aerosol particles by precipitation scavenging have been studied mainly by model simulations and laboratory experiments, but the results of these studies have not been fully examined by atmospheric observations. New particle formation from gas-to-particle conversion processes, including homogenous nucleation and subsequent particle growth, is an important source process to increase number concentration of aerosol particles with nanometer sizes. Nevertheless, the mechanism of new particle formation in the atmosphere has not been fully elucidated because of the complexity of the process and technical limitations of measurements. Number-size distributions of aerosol particles covering the size range below 100 nm diameter have been measured at various locations in the atmosphere since the development of new instruments during the 1990s. However, observations have seldom been made in the free troposphere over the East Asia and western Pacific area.

In this study, number-size distributions of aerosol particles of 9–300 nm diameters were observed at Mt. Norikura in central Japan during September 2001 and August–September 2002 (48 days in total). Two distinct air-masses transported from over the Pacific Ocean and continental Asia were observed during the observation periods. Discussion was focused on factors controlling variation of number-size distribution of free tropospheric aerosol particles observed at Mt. Norikura. Moreover, utilizing advantages of atmospheric conditions at Mt. Norikura, the observed size distributions were analyzed in terms of effects of precipitation scavenging and favorable conditions for new particle formation.

Observed number-size distributions of free tropospheric aerosol particles were compared with total precipitation amount in the air-masses for the last 24 hours (cumulative precipitation amounts). Cumulative precipitation amounts were estimated from the objective analysis data along air-mass backward trajectories. When cumulative precipitation amount increased from 0 to 20 mm, particle concentration of the Aitken mode range (9–100 nm in diameter) decreased by about half, and particle concentration of the accumulation mode range (100–300 nm in diameter) decreased by an order of magnitude. The cumulative precipitation amount is suggested as an important factor to modify the size distribution of free tropospheric aerosol at Mt. Norikura by decreasing particle concentration. From the relation between cumulative precipitation amount and particle concentration, the time constant of

precipitation scavenging for the particles in the accumulation-mode size range was estimated at the order of hours. The value estimated in this study agrees well with the time constant of in-cloud scavenging process estimated by model studies in literature, while the value estimated in this study is smaller than that of below-cloud scavenging process estimated by the model studies in literature by about two orders. These results suggest that in-cloud scavenging is important as a process controlling number-size distribution of free tropospheric aerosol particles at Mt. Norirkua

According to air-mass backward trajectories, observed air masses were classified into two types: the air mass transported from over the Pacific Ocean and the air mass transported from over continental Asia. Considering data for the air masses transported without precipitation, concentrations of accumulation mode particles (modal diameter about 100 nm) were almost identical (approximately 400 cm^{-3} as a median value) in the air masses transported from over the Pacific Ocean and continental Asia. Concentration of Aitken mode particles (modal diameter about 50 nm) in the air masses subsiding from over subtropical Pacific Ocean (890 cm^{-3} as a median value) was higher than that in the air masses transported from over continental Asia (230 cm^{-3} as a median value). Air-mass transportation pathway was found to be an important controlling factor for Aitken mode particle concentration in the free troposphere at Mt. Norikura.

Nucleation mode (a mode that first appears in the size range below 20-nm diameter) was observed on 4 days (called new particle formation (NPF) event days in this study) of 23 clear-sky days during the observation periods of this study. Occurrence of nucleation mode suggests new particle formation event occurred recently (in about a half day) in the observed air mass. Nucleation mode particles were observed in the mixed layer air transported by up-slope valley winds, but never in the free tropospheric air, suggesting that new particle formation event occurred in the air masses transported from the mixed layer.

SO_2, NH_3, and pre-existing particle concentrations observed in up-slope valley wind condition on NPF event days were compared with those on non-event sunny days. If H_2SO_4 or NH_3 were major precursors initiating homogenous nucleation and subsequent particle growth, high SO_2 or NH_3 concentration would be a favorable condition for new particle formation. However, this study found no positive correlation between an NPF event and SO_2 or NH_3 concentrations. On the other hand, homogenous nucleation competes with condensation onto pre-existing particles for low-volatile precursor gases; coagulation to pre-existing particles is a strong sink for freshly nucleated particles. Therefore, low pre-existing particle concentration is favorable condition for new particle formation. Based on the results of the observation at Mt. Norikura, pre-existing particle concentration on NPF event days was significantly lower than that on non-event sunny days. The average pre-existing particle concentration on NPF event days was about 50 % of that on non-event sunny days. This result suggests that low pre-existing particle concentration in the mixed layer is important for initiating a new particle formation event at Mt. Norikura.

This study investigated number-size distributions of submicron aerosol particles and factors controlling its temporal variation in the free troposphere over the East Asia and western Pacific area, where observation data have seldomly been obtained. Based on the results of the observation at Mt. Norikura, this study suggested a conceptual scheme of a cycle of number-size distribution of aerosol particles, relating to particle formation, growth, or removal processes in a Lagrangian perspective. Precipitation scavenging might be a key process for driving the cycle of size distribution of atmospheric aerosol particles.

1. Introduction

1.1. Atmospheric aerosol particles and their number-size distribution

Atmospheric aerosol particles affect the Earth's radiation balance and climate directly, by both absorbing and scattering incoming solar radiation, and indirectly, by acting as cloud condensation nuclei, thereby, modifying cloud properties [e.g., *Twomey*, 1977; *Charlson and Heintzenberg,* 1995; *Lohmann and Feichter,* 2005; *Yu et al.,* 2006]. However, current estimate of the aerosol effects contains a large uncertainty. The aerosol effects are crucially dependent on the aerosol properties: number-size distribution, chemical composition, and mixing state. These aerosol properties are highly variable in time and space in the troposphere because of patchy sources and sinks, and short residence time (days) [*Anderson et al.*, 2003], which complicates the estimate of the aerosol effects. To understand and predict variations of the aerosol properties in the atmosphere, factors controlling the variations must be understand in detail.

Number-size distribution of aerosol particles is the most important element describing atmospheric aerosol, as well as being a crucial parameter to estimate the aerosol effects on climate. Atmospheric aerosol have a continuous size distribution covering diameters from a few nm to several tens μm, which was shown by the pioneering study by *Junge* [1955]. *Whitby* [1978] showed that the size distribution of atmospheric aerosol particles is characterized by a multimodal distribution which can be approximated by the sum of log-normal functions. Typical modes appearing in the number-size distribution of atmospheric aerosol particles are called nucleation, Aitken, accumulation, and coarse modes [*Raes et al.*, 2000; *Kulmala et al.,* 2004]. Accumulation mode particles, which have a maximum concentration at the particle size of around 0.1 μm, are most effective for interacting with incoming visible solar radiation [*Seinfeld and Pandis,* 2006, Chap. 15]. Water-soluble particles in accumulation mode can be activated as cloud condensation nuclei under realistic

water vapor supersaturation in the atmosphere [*Pruppacher and Klett*, 1997, Chap. 6]. Coarse mode particles, which have a maximum concentration at particle size of around 1 μm, can also interact with visible solar radiation and be activated as cloud condensation nuclei in the atmosphere. However, total number concentration of coarse mode particles is much lower than that of the accumulation mode particles generally. Aitken and nucleation mode particles, which have maximum concentration at the diameters less than 0.1 μm, are less effective for climatic forcing.

Whitby [1978] suggested that the multimodal distribution results from mixture of aerosols with different formation mechanisms. Aerosol particles in coarse mode are formed mainly by disintegration processes of bulk material (e.g., sea salt and dust; *Whitby* [1978]); and aerosol particles composing nucleation, Aitken, and accumulation modes are formed mainly through gas-to-particle conversion processes or combustion processes. Although Aitken and nucleation mode particles are less effective for climatic forcing, the knowledge of the number-size distribution of Aitken and nucleation mode particles is important to elucidate the mechanisms to form accumulation mode particles in the atmosphere. The formation and growth processes of the submicron aerosol particles (accumulation, Aitken, and nucleation mode particles) in the atmosphere will be descried in detail in the following section.

1.2. Formation and growth processes of submicron aerosol particles

Homogeneous nucleation and subsequent particle growth is the process forming aerosol particles of nanometer sizes. When a strong new particle formation (NPF) event by homogeneous nucleation and subsequent particle growth processes occurs during atmospheric transport immediately before arrival at an observation site, a mode for particle diameter below about 20 nm, so-called nucleation mode is observed in number-size distribution of aerosol particles. The NPF events have been often observed in a various environments including the

free troposphere [e.g., *Clarke et al.,* 1998; *Lee et al.,* 2003], the continental boundary layer [e.g., *Mäkelä et al.,* 1997; *Weber et al.,* 1997; *Birmili* and *Wiedensohler*, 2000], coastal area [e.g., *O'Dowed et al.,* 1998], and urban area [e.g., *Stanier et al.*, 2004, *Wu et al.,* 2007]. The NPF is an important process to increase total aerosol particle concentration and eventually cloud condensation nuclei in the atmosphere [*Lihavainen et al.,* 2003; *Kerminen et al.,* 2005]. To estimate the formation rate of the aerosol particles, the mechanism of NPF and species participating in homogenous nucleation or subsequent growth of nucleated particles must be understood. Nevertheless, they have not been fully elucidated because of the complexity of the process and technical limitations of measurements [*Kulmala et al.*, 2004; *Holmes*, 2007].

Homogenous nucleation is the process that forms stable clusters of about 1-nm diameter from low-volatile vapors (condensable vapors). Homogenous nucleation in the atmosphere has been assumed to occur by several mechanisms: binary nucleation of H_2SO_4-H_2O vapors [e.g., *Kulmala et al.*, 1998; *Noppel et al.*, 2002; *Berndt et al.,* 2005; *Yu,* 2006a], ternary nucleation of H_2SO_4-H_2O-NH_3 vapors [e.g., *Ball et al.*, 1999; *Korhonen et al.*, 1999; *Napari et al.*, 2002], nucleation enhanced by organic vapors (H_2SO_4-H_2O-organic) [*O'Dowd et al.*, 2002a; *Zhan et al.,* 2004], and ion-induced nucleation (H_2SO_4-H_2O-ion) [e.g., *Yu and Turco*, 2000; *Yu*, 2006b]. Species participating in homogenous nucleation process can be different from the major chemical components of atmospheric aerosol particles since the species participating in homogenous nucleation and following growth processes can differ. Commonly, NPF events in the lower troposphere have been assumed to occur through ternary nucleation involving H_2SO_4-H_2O-NH_3 vapors. However reliable model to predict nucleation rate of H_2SO_4-H_2O-NH_3 vapors nucleation does not currently exist [*Attila et al.,* 2005; *Yu,* 2006c].

Homogenous nucleation competes with condensation onto pre-existing particles for condensable vapors; coagulation to pre-existing particles is a strong sink for freshly nucleated

stable clusters with diameters of a few nanometers [*Kerminen et al.*, 2001]. Therefore, high pre-existing particle concentration is an unfavorable condition for NPF events. In the condition of high pre-existing particle concentration, strong sources of condensable vapors exceeding the negative effects of pre-existing particles are necessary for initiating an NPF event.

Freshly nucleated particles of a few nm sizes are scavenged rapidly by coagulation to pre-existing particles although the scavenging speed decreases as the small particles grow in size, because coagulation coefficient is much larger for particles of different sizes than for particles of similar sizes. The coagulation rate, J_{ij} of the aerosol particles with different diameters D_i and D_j is expressed by the following equation:

$$J_{ij} = K_{ij} N_i N_j, \tag{1-1}$$

where N_i and N_j is number concentrations of particles with diameters D_i and D_j, and K_{ij} is the coagulation coefficient. Fig. 1-1 shows the Brownian coagulation coefficient K_{ij} ($cm^3 \cdot s^{-1}$) for coagulation of particles of diameters D_i and D_j in air at 297 K and1013 hPa calculated by the equation of *Fuchs* [1964] (summarized in *Seinfeld and Pandis* [2006], Table 13.1). *Kulmala et al.* [2000] hypothesized that the key process controlling occurrence of NPF events is not homogenous nucleation but competition of size growth of freshly nucleated particles and scavenging of them by coagulation to pre-existing particles. To understand NPF process, particles growth following homogenous nucleation might be an important process as well as homogenous nucleation.

Typical growth rates during NPF events are 1–20 $nm \cdot h^{-1}$ for remote and polluted environments in the lower troposphere [*Kulmala et al.*, 2004]. Particle growth by self-coagulation of newly formed particles is too slow to explain the observed growth rates. The growth rate by self-coagulation of mono-dispersed aerosol particles can be estimated

using the following equation:

$$\frac{dD_p}{dt} = \frac{D_p KN}{6}. \qquad (1\text{-}2)$$

For a mono-dispersed aerosol of particle diameter D_p =10 nm (coagulation coefficient K=1.4×10^{-9} cm^3·s^{-1} for parameter values in Fig. 1-1) and particle number concentration N=10^4 cm^{-3} (an upper estimate), particle growth rate by self-coagulation is estimated at about 0.5 nm·h^{-1}, which is lower than the typical growth rate observed during NPF events. Therefore, particle growth is considered to be caused mainly by condensation of low-volatility vapors. Gas-phase H_2SO_4 concentration is often insufficient to explain the observed particle growth rates, suggesting the contribution of condensable vapors other than H_2SO_4 [e.g., *Birmili et al.*, 2003; *Boy et al.*, 2005]. Over the boreal forests of northern Europe, it is believed that oxidation products of biological volatile organic compounds contribute greatly to the growth of freshly formed particles [e.g., *O'Dowd et al.*, 2002b; *Tunved et al.*, 2006].

The nucleation mode particles grow into Aitken mode particles with diameters of several tens to 100 nm by condensation of low-volatile vapors, and subsequently into accumulation mode particles. For larger Aitken mode particles, the aqueous phase oxidation of SO_2 in cloud droplets in non-precipitating clouds may serve an effective path of growing into accumulation mode particle [*Hoppel et al.,* 1986; *Hoppel et al.,* 1994a, 1994b]. The speed of particle growth after new particle formation might depend on the amount of available precursor-gases and frequency of cloud processing during air-mass transportation.

1.3. Removal processes of submicron aerosol particles

The shape of the number-size distribution of atmospheric aerosol particles is modified by particle removal processes as well as by particle formation and growth processes. The processes that can reduce the number concentration of atmospheric aerosol particles are

coagulation, and deposition on the Earth's surface. Total volume concentration of aerosol particles does not change by coagulation while number concentration is reduced. On the other hand, both of number and volume concentration of aerosol particles are reduced by the deposition process. Submicron particles deposit on the Earth's surface mainly by wet deposition; because gravitational settling is very slow for submicron particles, thus they do not deposit effectively by dry deposition [*Seinfeld and Pandis,* 2006, Chap. 20].

The equation describing evolution of the number-size distribution of aerosol particles by coagulation (*Seinfeld and Pandis* [2006], the equation 13.59 or 13.61) can not be solved analytically. However, assuming that the coagulation coefficient K_{ij} is constant (K), the evolution of total particle number concentration, N_T is given by an analytically soluble equation,

$$\frac{dN_T}{dt} = -\frac{1}{2} K N_T{}^2(t) . \qquad (1\text{-}3)$$

If $N_T(0)=N_0$, the solution of (1-3) is

$$\frac{1}{N_T(t)} - \frac{1}{N_0} = \frac{Kt}{2} \quad . \qquad (1\text{-}4)$$

Figure 1-2 shows temporal variation of particle number concentration, as predicted by the equation 1-4 for a coagulation coefficient of 3×10^9 $cm^3 \cdot s^{-1}$, which corresponds to average K of a log normally distributed aerosol with geometric mean diameter 50 nm and geometric standard deviation 1.5 under the standard conditions [*Lee and Chen*, 1984]. This figure shows that coagulation will have a small effect on particle number concentration for the concentrations below about 10^3 cm^{-3} in the period of days.

As for the scavenging processes of aerosol particles by precipitation (precipitation scavenging), an aerosol particle can be incorporated into a rain drop by one of the following processes: (1) Aerosol particle becomes a cloud droplet (~ 10 μm diameter) by nucleation

scavenging and grows into a rain droplet (~ 0.1–5 mm diameter) by collision and coalescence with other cloud droplets, (2) Aerosol particle becomes a cloud droplet by nucleation scavenging in cloud and is collected by collision with a falling raindrop in cloud, (3) aerosol particle becomes cloud interstitial aerosol (aerosol particles not serving as cloud or ice nucleus and remaining at below 1 μm diameter in cloud) and collected by collision with a cloud droplet or a rain droplets in cloud, (4) Aerosol particle is collected by a falling droplets below cloud. The processes (1), (2), and (3) can occur together in cloud and are referred as in-cloud scavenging. On the other hand, only the process (4) occurs below cloud, which is referred as below-cloud scavenging.

In-cloud scavenging involves both of nucleation and impaction scavenging, while below-cloud scavenging involves only impaction scavenging. Nucleation scavenging occurs in the initial stage of cloud formation; aerosol particles that are active as cloud condensation nuclei or ice nuclei are incorporated into cloud droplets by this scavenging process. Impaction scavenging is the process incorporating aerosol particles into cloud or precipitation hydrometeors by the various forces as following: Brownian diffusion, interception, inertial impaction, thermophoresis, diffusionphoresis, airflow turbulence and electronic attraction [*Pruppacher and Klett,* 1997, Chap. 17, for a detailed review]. *Greenfield* [1957] showed that efficiencies of impaction scavenging is high for very small (below about 10 nm in diameter) and large (above about 2 μm in diameter) aerosol particles because of Brownian motion for the very small particles and large inertia for the large particles. On the other hand, for the aerosol particles with diameters between 10 nm and 2 μm, efficiencies of impaction scavenging were found to be very low. The size range with low efficiency of impaction scavenging, which is sometimes referred as the "*Greenfied gap*", corresponds to the sizes of Aitken and accumulation mode particles. Therefore, below-cloud scavenging might not be effective for Aitken and accumulation mode particles. For accumulation mode particle that

can act as cloud condensation nuclei, in-cloud scavenging might be the dominant removal process. In addition, although Aitken mode particles are less active as cloud condensation nuclei, they might be removed by collision with cloud droplets in cloud.

Collision efficiency, E (D_{rain}, D_{p}) is the ratio of the total number of collisions occurring between a rain droplet of diameter D_{rain} and aerosol particles to the total number of aerosol particles in an area equal to the raindrop's effective cross-sectional area. Figure 1-3 shows collision efficiency, E, between a raindrop of diameter 0.1 mm and an aerosol particle of diameter D_{p}. The relation of D_{p} and E was calculated by the equation proposed by *Slinn* [1983] (summarized in *Seinfeld and Pandis* [2006], p. 950), which was obtained by a dimensional analysis coupled with experimental data.

Λ (D_{p}) is the rate of removal of aerosol particles of diameter D_{p} by rain with a raindrop size distribution. Below-cloud scavenging rate of aerosol particles of diameter D_{p} is given by the equation:

$$\frac{dN(D_p)}{dt} = -\Lambda(D_p)N(D_p), \qquad (1\text{-}5)$$

where $N(D_{\mathrm{p}})$ is the number concentration of aerosol particles of diameter D_{p}.The below-cloud scavenging coefficient, Λ (D_{p}) is written as

$$\Lambda(D_p) = \int_0^\infty \frac{\pi}{4} {D_{rain}}^2 U_t(D_{rain}) E(D_p, D_{rain}) N_{rain}(D_{rain}) dD_{rain} \quad , \qquad (1\text{-}6)$$

where U_t is the raindrop terminal velocity, and N_{rain} (D_{rain}) is the raindrop size distribution. Based on the equation 1-6, Λ (D_{p}) can be estimated assuming a raindrop size distribution. The characteristic time (e-folding time), τ (D_{p}) of below-cloud scavenging for the particles of diameter D_{p} is

$$\tau(D_p) = \frac{1}{\Lambda(D_p)}. \qquad (1\text{-}7)$$

Λ (D_p) and τ (D_p) calculated for the precipitation rate, 1 mm·hr^{-1} are shown in Fig. 1-3a and b respectively. Figures 1-4 shows (a) Λ (D_p) and (b) τ (D_p) for the raindrop size distribution of Marshall and Palmer (1948) with various precipitation rates.

Many model studies and laboratory experiments have been dedicated to determine the collision efficiency, E, or the scavenging coefficient, Λ (D_p) [e.g., *Wang et al.,* 1978; *Grover et al.,* 1977; *Wang and Pruppacher*, 1977; *Scott*, 1982; *Slinn,* 1983; *Mircea and Stefa*n, 1998]. However, the parameterizations of the scavenging coefficient have seldom been tested by field experiments by observing particle number-size distributions; although the bulk-mass scavenging coefficients have been estimated from the mass concentrations of chemical species observed in precipitation waters and aerosol particles [e.g., *Okita et al.,* 1996; *Andronache,* 2004].

1.4. Advantages in the atmospheric observation at mountain site

Because most of primary particles and precursor gases of secondary particles are emitted from near the Earth's surface, the free tropospheric aerosol might be less influenced by local particles sources compared with the boundary layer aerosol. Thus, the free tropospheric aerosol might be suitable to investigate effects of air-mass histories, such as air-mass transportation pathways and meteorology during air-mass transportation, on aerosol properties. Free tropospheric aerosol can be observed using the air craft, but the aircraft-borne observation is not suitable to long-term continuous observations. The high-elevation mountain site are available for a long-term continuous observation of the free tropospheric aerosol that is long enough to observe various air-masses having different transportation or meteorological histories, which might help us to understand influences of the air-mass histories on aerosol properties.

As a mountain-based long-term observation of free tropospheric aerosols, *Raes et al.*

[1997] observed number-size distributions of free tropospheric aerosol particles with diameters of 16–620 nm at the Canary Islands in the northeast Atlantic, and showed average size distributions in a continental air mass transported from northern Africa and a marine air mass subsiding from over the northern Atlantic Ocean. *Weingartner et al.* [1999] showed average number-size distributions of aerosol particles with diameters of 10–750 nm at Jungfraujoch in the Swiss Alps, and asserted a difference of the average size distribution among seasons. However, modification of the size distribution by meteorology such as cloud and precipitation during air transportation was not considered in those studies.

A local wind system including upslope valley wind and down-slope mountain winds has been recognized at high-elevation mountain sites [*Mendonca,* 1969; *Lugauer et al.,* 1998; *Nyeki et al.,* 1998]. Down-slope mountain winds are caused by radiative cooling of the mountain surface during the nighttime [*Barry,* 1992]; the winds transport the free tropospheric air above the observation site. Up-slope valley winds result from solar heating of mountain surfaces during the daytime; the winds transport the boundary air to the observation site. The boundary layer air transported by up-slope winds prevents observation of free tropospheric during the daytime at high-elevation sites. Thus, most of free tropospheric aerosol observations at high-elevation sites have been carried out during the nighttime. On the other hand, the diurnal variation of the local wind system might be useful to observe the aerosols transported from both of the free troposphere and the boundary layer.

The several field studies at near-surface sites have pointed out a relationship between new particle formation (NPF) events and micrometeorology within the boundary layer. *Nilsson et al.* [2001a] showed that the onset of an NPF event correlates well with the onset of turbulence in the boundary layer. *Buzorius et al*. [2001] and *Held et al.* [2004] observed the downward flux of freshly formed particles using the eddy covariance method above the forest canopy during NPF events, implying that particle sources exist above the forest canopy.

Although some measurements have been made using a tethered balloon [*Stratmann et al.*, 2003; *Siebert et al.,* 2004; *Wehner et al.*, 2007] and airplanes [e.g., *Keil and Weidenhoser*, 2001; *McNaughton et al.*, 2004], vertical distributions of parameters related to NPF, such as concentrations of freshly formed and pre-existing particles and precursor gases, have seldom been measured for the boundary layer and lowermost free troposphere during NPF events. The diurnal evolution of aerosols relating with the local wind system at the high-elevation site might provide us a clue to the vertical extent of NPF event in the lower troposphere.

1.5. Seasonal change of air mass transportation pathway over Japan

Relating to the seasonal change of synoptic wind patterns around Japan, the free troposphere over central Japan is covered by two distinct air masses: sub-tropical marine air mass transported from over the Pacific Ocean and continental air mass transported from over continental Asia. In summer, the dominant air mass is the marine air mass over Japan, but it yields to the continental air mass during other seasons. Associated with the seasonal changes of air-mass transportation pathway, clear seasonal variation has been observed in aerosol optical properties and particle shape [*Sakai et al.,* 2000], ionic constituents of aerosol particles [*Osada et al*., 2002], and aerosol particle concentrations at $D_p > 0.3$ μm [*Osada et al.*, 2003] in the free troposphere over central Japan. Long-term continues observations of free tropospheric aerosol size distribution covering the diameters of the Aitken and nucleation modes particles have not been made for the western Pacific area. A few campaign studies by aircraft-borne observations have been reported for aerosol number-size distribution for the free troposphere near Japan [*Zaizen et al.*, 2004; *McNaughton et al.*, 2004], but these are short-term case studies that fail to provide reliable parameters of size distribution representing this region.

1.6. Objectives of this study

This study observes temporal variation of the particle size distribution covering the diameters of nucleation, Aitken, and accumulation mode particles (9–300 nm) at a high-elevation mountain site, Mt. Norikura (2770 m a.s.l.) in central Japan with the main purpose of finding out the important factors that control temporal evolution of number-size distributions of submicron aerosol particles at Mt. Norikura. Experimental details about the aerosol observation at Mt. Norikura and analytical methods are described in Chapter 2. Temporal variation of the particle size distribution of the free tropospheric aerosols at Mt. Norikura and discussions about effects of precipitation during air-mass transportation and air-mass transportation pathways are described in Chapter 3. Chapter 4 focuses on occurrence of nucleation mode in number-size distributions of aerosol particles and discusses about favorable atmospheric condition for occurrence of nucleation mode particles at Mt. Norikura. Finally, factors controlling the variation of the number-size distribution of submicron aerosol particles in the atmosphere are discussed in Chapter 5.

2. Experiments

2.1. Atmospheric observation at Mt. Norikura

Aerosol observations were performed at the Norikura Observatory (36.1°N, 137.5°E, 2770 m a.s.l.) of the Institute for Cosmic Ray Research (ICRR), University of Tokyo, near the top of Mt. Norikura (summit elevation 3026 m a.s.l.) in central Japan (Fig. 2-1). The observatory is above the forest limit in a preserved area, a national park, and is isolated from industrial urban areas. The nearest cities are Takayama and Matsumoto, which are cities of 100,000–200,000 people at a distance of 30–40 km from the observatory. The observatory is above the forest limit and is in an alpine belt in which dwarf Siberian pine (*Pinus pumila*) scrub is distributed. Conifers and *Betula ermanii* are dominant in the subalpine belt (1500–2500 m a.s.l.) and deciduous broadleaf trees such as Japanese beech and oaks are dominant in the montane belt (< 1500 m a.s.l.) in the mountain area in central Japan. Observation periods are 22–30 September 2001, 29 July–23 August 2002, and 10–27 September 2002 (48 days in all). The observation period, which includes a transition period between summer and autumn, was selected to observe the two contrasting major air masses for Japan transported from the Pacific Ocean and continental Asia.

2.2. Instrumentation

(i) Particle number-size distribution

Number–size distributions of 9–300 nm diameter particles were measured using a Scanning Mobility Particle Sizer (SMPS; TSI Inc.) including a DMA (Electrostatic Classifier 3071A; TSI Inc.) and a condensation particle counter (UCPC3025A; TSI Inc.). Sample air was drawn into the instrument from an inlet 2 m above the ground through a 2-m electrically conductive silicone rubber tube. Particle losses onto the sampling tube were corrected using laminar flow diffusion theory [*Hinds,* 1999]. During the observation period of September

2001, the sheath air of the DMA was not dehumidified with desiccants and the relative humidity (RH) of the sheath air was therefore almost equal to that of the laboratory room air. During the observation periods of August–September 2002, the relative humidity of the sheath air was kept under 20% using desiccants to measure the dry particle size. For the analysis described in Chapter 3, only data that were measured in August–September 2002 were used. Commercial software (TSI, Inc.) was used for data acquisition and conversion from the particle mobility distribution to the particle size distribution. Particle size distribution data were obtained every 3 min (150 s for data scan followed by a 30 s down time). The particle number concentrations presented in this paper are corrected to a 1013 hPa condition from the 725 hPa condition where the observatory is located.

(ii) SO_2, NH_3 and O_3 concentrations

In the observation period during September 2001 (8 days), the SO_2 and NH_3 concentrations were measured continuously using alkaline (1% Na_2CO_3 in a 1% glycerol solution by mass) and acid (0.01 M oxalic acid in a 16/84 glycerol/methanol solution by volume)-impregnated cellulose filters. The impregnated filters were set in a 47-mm stacked filter pack (NILU) with a Teflon membrane filter before the impregnated filters to remove particulate matter. The sampling period per sample was 6–10 hours during the nighttime and 3–6 hours during the daytime. The concentrations of SO_2 and NH_3 collected on the impregnated filters were analyzed using ion chromatography. More details of SO_2 and NH_3 sampling using the impregnated filters and the chemical analysis were given by Kido et al. [2001] and Kido [2001]. For the observation periods of August –September 2002 (40 days), SO_2 concentrations were measured continuously using a pulsed UV fluorescence SO_2 analyzer (Model 43C-Trace Level; Thermo Electron Corp.). The NH_3 concentration for this season was also measured using acid-impregnated filters for intensive observation periods (29 July–1 August, 21– 22 August, and 22–26 September 2002). Ozone (O_3) concentrations were

measured using a Dasibi-type UV absorption O_3 monitor (Model 1150; Tokyo Dylec Corp.).

(iii) Meteorological parameters

Local meteorological parameters (wind direction, wind speed, ambient air temperature, and precipitation rate) were measured using a Mini-met weather station (Grant Instruments). Dew point temperatures were measured with an impedance hygrometer (Cermet II; Michell Instruments Ltd.). Vertical profiles of air temperature and relative humidity were obtained from the sounding performed regularly by the Japan Meteorological Agency at Wajima, approximately 150 km NNE of Mt. Norikura (see Fig. 2-1 for the site location).

2.3. Data screening

The observatory is situated between mountains to the south and north (Fig. 2-2). Therefore, the local wind directions are limited mostly to east and west. Possible local air pollution sources include exhaust of diesel power generators located east of the observation laboratory. No discernible local air pollution source is located west of the laboratory. Therefore, the influence of the local air contaminants was eliminated from aerosol data according to local wind direction.

The 3-min size distribution data were screened in reference to local wind direction to remove local air contamination from the data. Fig. 2-3 shows examples of 3-min data (number concentration of 9–33 nm diameter particles) (a) before and (b) after the elimination of influence of local air contamination. About 80% of 3-min data were retained after the contamination screening. The hourly size distribution was calculated if more than five 3-min raw data were retained after the contamination screening for that hour.

2.4. Analytical methods

(i) Log-normal fitting

Hourly number-size distributions of aerosol particles were approximated by a sum of up to three log-normal functions individually. The sum of the log-normal function is given as:

$$\frac{dN}{d\log D_p} = \sum_{i=1}^{n} \frac{N_i}{\sqrt{2\pi}\log\sigma_{g,i}} \exp\left[-\frac{\left(\log D_p - \log D_{g,p,i}\right)^2}{2\log^2\sigma_{g,i}}\right] . \qquad (2\text{-}1)$$

Therein, D_p is the particle diameter, n is the number of modes, $D_{g,p,i}$ is the modal geometric mean diameter, $\sigma_{g,i}$ is the modal geometric standard deviation, and N_i is the particle number concentration in mode i. Details of the log-normal distribution are described by *Seinfeld and Pandi*s [2006, Chp.8]. These modal parameters were obtained using a nonlinear peak-fitting tool that was included with commercial software (Origin; OriginLab Corp.). We applied the restrictions as (1) N_i > 1% of total particle concentration and N_i > 1 cm^{-3}, (2) 1.3 $D_{p,g,1} < D_{p,g,2}$, (3) $\log\sigma_{g,i}$ < 0.5 to avoid unrealistic mode fitting. Generally, according to their geometric mean diameter, modes appearing in sub-micrometer sizes are called nucleation, Aitken, and accumulation modes [*Raes et al.,* 2000; *Kulmala et al.,* 2004]. In Chapter 3, I follow the names of modes in sub-micrometer sizes: nucleation mode, $D_{p,g}$ < 30 nm; Aitken mode, 30 nm < $D_{p,g}$ < 85 nm; and accumulation mode, $D_{g.p}$ > 85 nm. The borders of size ranges among nucleation, Aitken, accumulation modes were set to reduce the number of data of multi-modes in the size range to a minimum. In addition, N_i of each mode is called nucleation, Aitken, and accumulation mode concentration in this study.

(ii) Condensation sink

The condensation sink (*CS*) is a measure of the scavenging speed of gaseous molecules caused by condensation onto particles, which depends strongly on the particle size and concentration. Actually, *CS* is calculated using the following equation [*Kulmala et al.,* 2001].

$$CS = 2\pi D_v \int_0^\infty D_p \beta_m(D_p) N(D_p) dD_p \\ = 2\pi D_v \sum_i D_{p,i} \beta_{m,i} N_i \quad . \tag{2-2}$$

In that equation, D_v is the diffusion coefficient of the condensing vapor. The diffusion coefficient of H_2SO_4 vapor (0.077 $cm^2 \cdot s^{-1}$ [*Hanson and Eisele,* 2000]) is used for calculations. In addition, $D_{p,i}$ and N_i respectively denote the particle diameter and number concentration of size class *i*. The transitional correction factor $\beta_{m,i}$ can be expressed by [*Fuchs and Sutugin,* 1971]

$$\beta_{m,i} = \frac{Kn_i + 1}{0.377 Kn_i + 1 + \frac{4}{3}\alpha^{-1} Kn_i^{\,2} + \frac{4}{3}\alpha^{-1} Kn_i} \quad , \tag{2-3}$$

where the mass accommodation coefficient α is assumed as unity. The Knudsen number is

$$Kn_i = \frac{2\lambda_v}{D_{p,i}} \, . \tag{2-4}$$

λ_v is the mean free path of condensing vapor molecule which is expressed by

$$\lambda_v = 3D_v \sqrt{\frac{\pi M_v}{8 K_B T}} \, . \tag{2-5}$$

M_v is the molecular mass of the condensing vapor, K_B is Boltzmann constant, and T is air temperature.

To include particles that are larger than our detection limit (300 nm diameter), *CS* was calculated from the particle size distributions reproduced from the log-normal distribution parameters that were obtained by fitting to observed particle size distributions. Particles of the mode with geometric mean diameter larger than our instrumental limitation (e.g. coarse mode particles) and the effect of hygroscopic growth of particle size in ambient air were not considered. However, coarse mode particles might not cause a major error (< ca. 10 %) in the

CS calculations because the concentrations of coarse particles (D_p >1μm) normally observed at Mt. Norikura are low (ca. 10^{-1} cm^{-3}) [*Osada et al.,* 2007]. On the other hand, effects of hygroscopic growth can result in a significant underestimation (up to several hundred percent) of *CS* in ambient air.

(iii) Concentration and production rate of condensable vapor

Assuming that the pressure of the saturated condensing vapor is zero, the particle growth rate dD_p/dt can be expressed as the following equation [*Kulmala et al.,* 2001]:

$$\frac{dD_p}{dt} = \frac{4m_v \beta_m D_v C_v}{\rho D_p}. \qquad (2\text{-}6)$$

Thereby, m_v is the molecular mass of the condensing vapor, C_v is the condensing vapor's concentration, and ρ is the particle density. C_v can be estimated by integrating the equation (2-6) from D_{p0} to D_p assuming that C_v is constant during particle growth [*Kulmala et al.*, 2001]:

$$C_v = \frac{\rho}{\Delta t D_v M_v} \times \left[\frac{D_p{}^2 - D_{p0}{}^2}{8} + \left(\frac{4}{3\alpha} - 0.623 \right) \frac{\lambda_v}{2} \left(D_p - D_{p0} \right) + 0.623 \lambda_v{}^2 \ln \frac{2\lambda_v + D_p}{2\lambda_v + D_{p0}} \right] \qquad (2\text{-}7)$$

We took the diffusion coefficient of H_2SO_4 to estimate C_v, although condensing species contributing to particle growth are unknown. On the other hand, we took the particle density of ammonium sulfate (1.77 $g \cdot cm^{-3}$ [*International Critical Tables*, 1928]) assuming that each H_2SO_4 molecule is neutralized by two NH_3 molecules in particles because the NH_3 concentration is presumed to be much higher than the gas-phase H_2SO_4 concentration.

A balance equation for condensable vapor is

$$\frac{dC_v}{dt} = Q - CS \times C_v, \tag{2-8}$$

in which Q is the source rate of the condensable vapor. Assuming a pseudo-steady state, Q can be estimated using the following equation:

$$Q = CS \times C_v. \tag{2-9}$$

2.5. Air-mass backward trajectory

Backward trajectories were computed using the Hybrid Single-Particle Lagrangian Integrated Trajectory (HYSPLIT) model developed by NOAA ARL [*Draxler and Rolph,* 2003; *Rolph,* 2003]. The National Weather Service's National Centers for Environmental Prediction (NCEP) FNL archive was used for meteorological input data. Vertical wind velocities were used to calculate vertical motions of air parcels.

3. Number-size distributions of free tropospheric aerosol particles observed at Mt. Norikura: Effects of precipitation and air-mass transportation pathway

This chapter presents temporal variation of the particle size distribution of the free tropospheric aerosols observed at Mt. Norikura and discusses about effects of precipitation during air-mass transportation and air-mass transportation pathways. In section 3-1, influences of the local wind system are examined to select data of free tropospheric aerosol. In section 3-2, to investigate effects of air-mass transportation pathways on aerosol size distribution, the observed air-masses are classified into two types according to their backward trajectories. Temporal variation of number-size distributions of free tropospheric aerosol particles is compared with cumulative precipitation amounts during the preceding 24-hours in Section 3-3. Relations of number concentrations of aerosol particles with cumulative precipitation are shown in Section 3-4, and scavenging coefficients by precipitation scavenging are estimated from the results of the observation. In Section 3-5, the number-size distributions observed in the air-masses transported from over the Pacific Ocean and continental Asia with and without precipitation are compared.

3.1. Local wind system: Down-slope mountain and up-slope valley winds

As mentioned in section 1-4, the boundary layer air transported by upslope valley winds prevents the observation of free tropospheric air at the high-elevation site during the daytime. As a tracer of the lower boundary layer air, the SO_2 concentration might be a suitable parameter. In general, SO_2 concentration levels decrease with increasing altitude and are different between boundary layer and free troposphere [*Warneck,* 1999]. Figure 3-1 shows average diurnal variation of normalized SO_2 concentrations of clear summer days (6 days during the period from 29 July to 8 August 2002). The SO_2 concentrations were normalized:

daily average values were made unity. The SO_2 concentration showed clear diurnal variation: an increase in daytime and a decrease during nighttime. Lowest SO_2 concentrations were observed during 23:00–7:00 local time (LT, UT+9 h), associated with down-slope mountain winds during nighttime. In this chapter, aerosol data during 0:00–6:00 LT are discussed as containing free tropospheric aerosols.

3.2. Air-mass transportation pathway and meteorological condition

Air mass backward trajectories for five days were analyzed to investigate their relation to observed size distributions of aerosol particles. Calculations of backward trajectories were begun from 3000 m a.s.l., 230 m above the site at 1 h, 3 h, and 5 h LT. According to the backward trajectories, transportation pathways of observed air masses were classified into two groups: type A, transported from the Pacific Ocean; and type B, transported from other areas. Air masses were classified as type A if the endpoint of five-day backward trajectory was located at above the Pacific Ocean without passing over continental Asia. Air masses that did not meet conditions of type A were classified as type B. Figures 3-2a and 3-2b show backward trajectories classified respectively into types A and B. Figure 3-2b shows that almost all air masses of type B were transported from continental Asia and that several air masses stagnated near Japan.

Figure 3-3 shows the respective variations of (a) ambient air and dew point temperatures, (b) O_3 concentrations, and (c) local precipitation rate. The parameters in Fig. 3-3 are average values in free tropospheric conditions (0–6 h LT) except for local precipitation rates ($mm \cdot h^{-1}$) of 0–6 h LT. The air-mass transportation patterns, types A and B, are indicated at the top of Fig. 3-3a by black and gray bars. For the period when aerosol data were not obtained, classification of the transportation pattern is not shown at the top of Fig. 3-3a.

Air and dew point temperatures were constantly high in type A, but variable in type B

(Fig. 3-3a). Low O_3 concentrations (10–30 ppb) were observed in type A (Fig. 3-3b). In type B, consisting mostly of the air masses from continental Asia, O_3 concentration levels were higher (20–60 ppb) than those in type A. The difference in the O_3 concentrations between the air mass types might result from origin and air-mass transportation pathway. Low O_3 concentrations are thought to be characteristic of a clean marine troposphere. At the summit of Mt. Fuji (35.4°N, 138.7°E, 3776 m a.s.l.) in Japan [*Tsutsumi et al*., 1998] and over the western Pacific Ocean [*Tsutsumi et al*., 1996], lower O_3 concentrations (ca. 20 ppb) have been reported for marine air masses transported from over the Pacific Ocean, although high O_3 concentrations (40–50 ppb) have been reported for air masses transported from continental Asia. Therefore, low O_3 concentrations in type A (10–30 ppb) and high O_3 concentrations in type B (20–60 ppb) are consistent with the low concentrations reported in clean marine air masses in the western Pacific area and high concentrations for air mass from continental Asia.

Figure 3-4 shows the 700 hPa geopotential height field on 6 August 2002 as a representative synoptic-scale meteorological condition of type A, which is frequently observed in summer months in Japan. Figure 3-4 shows that when an air mass was transported from the Pacific Ocean to Mt. Norikura, central Japan was covered by a Pacific high-pressure system centered over the northwestern Pacific Ocean. In contrast, various patterns of synoptic-scale meteorological conditions existed for the type B air mass. As examples of meteorological patterns of type B, Fig. 3-5 shows 700 hPa geopotential height fields on (a) 1 August (b) 24 September, and (c) 17 September 2002. As described above, air and dew point temperatures were variable in type B (Fig. 3-3a). The variations of air and dew point temperatures are apparently related to the variation of synoptic-scale meteorological condition of type B. For example, high air and dew point temperatures were often observed when a Pacific high-pressure system was located over western and central Japan, as shown in Fig. 3-5a. Figure 3-5b shows that low air and dew point temperatures were often observed when

central Japan was under the influence of mid-latitudinal westerly winds. Local precipitation was observed frequently from 11–18 September (Fig. 3-5c). Figure 3-5c shows that these local precipitation events were mainly brought by synoptic frontal systems, so-called Shurin, located near central Japan.

In all cases, SO_2 concentrations (not shown in Fig. 3-3) were below or close to the detection limit of the SO_2 analyzer (ca. 0.1 ppbv) in the free tropospheric air condition. Several active volcanoes emit large amounts of volcanic gases in Japan (e.g., Miyakejima Volcano [*Kajino et al.,* 2004] and Mt. Asama [*Andres and Kasgnoc*, 1998]). However, the low SO_2 concentrations suggest that the observed aerosols were not influenced by the active volcanoes nearby.

3.3. Variations of number-size distribution of free tropospheric aerosol particles and cumulative precipitation amount

Figure 3-6 shows temporal variations of (a) number-size distribution ($dN/d\log D_p$, cm^{-3}) of aerosol particles observed in free tropospheric conditions (0–6 h LT), (b) modal geometric mean diameters ($D_{p,g,i}$) obtained by log-normal fitting, (c) particle number concentrations in each mode and total particle concentrations of 9 nm < D_p < 300 nm ($N_{9–300}$), and (d) the cumulative precipitation amount experienced by air mass for the preceding 24 h. The air-mass transportation patterns, types A and B, are indicated at the top of Fig. 3-6a. Aerosol data were not obtained on the days indicated as “no data” in Figs. 3-6a and 3-6c either because of failure in data acquisition or local air contamination.

Parameters of precipitation scavenging on aerosol particle concentration include the magnitude and duration of precipitation experienced by the observed air mass before arrival. Thus, cumulative precipitation amounts in the air mass might be a useful parameter to evaluate effects of precipitation scavenging on the concentration and size distribution of

aerosol particles. The cumulative precipitation amount shown in Fig. 3-6d was estimated for the 24 h before arrival based on hourly precipitation rates along backward trajectories obtained using the HYSPLIT model. Although the meteorological parameters obtained using the HYSPLIT model are not observed data but objective analytical data, these values can be useful for diagnosing meteorological conditions along the trajectory.

Throughout the observations, accumulation and Aitken modes were dominant over nucleation modes in both frequency of occurrence (FO) and modal concentration (Fig. 3-6c). About 50% of the observed size distributions were bimodal distributions with accumulation and Aitken modes, and about 40% were mono-modal distributions of either accumulation or Aitken modes.

During 6–20 August (predominantly type A), large variations of $N_{9–300}$ and size distribution were observed (Fig. 3-6c). Note that low $N_{9–300}$ were observed in the air mass with higher cumulative precipitation amount (e.g., 9–10 and 14–15 August). In contrast, lower cumulative precipitation amounts might engender higher $N_{9–300}$ concentrations with large variability. In addition, accumulation-mode concentrations were extremely low during a severe local precipitation event (12–18 September in Fig. 3-3c). Thus, precipitation scavenging is an important controlling factor of aerosol concentration, especially for accumulation mode particles. In other words, precipitation scavenging might modify the aerosol particles' size distribution.

3.4. Relationship between precipitation amount and particle number concentration

Figure 3-7 depicts the relationship between particle concentration and cumulative precipitation amounts for the last 24 h in air mass: (a) total particle concentration in sizes of 9 nm < D_p < 100 nm ($N_{9–100}$) and (b) total particle concentration in sizes of 100 nm < D_p < 300 nm ($N_{100–300}$) to the cumulative precipitation amount. Negative correlations of the logarithm

of $N_{9–100}$ and $N_{100–300}$ with cumulative precipitation amounts are shown respectively in Figs. 3-7a and 3-7b. Least-squares fitting lines using the exponential function are also shown in Fig. 3-7. The fitting lines indicate that when the cumulative precipitation amount was increased from 0 mm to 20 mm, $N_{9–100}$ was decreased by about half (Fig. 3-7a) and $N_{100–300}$ was decreased by an order of magnitude (Fig. 3-7b). Although the coefficients of determination (R^2) of the fitting line are especially low for the fitting line in Fig. 3-7a (0.08), the correlations shown respectively in Fig. 3-7a and 3-7b are statistically significant at the 0.01 level.

For comparison of our results with other studies, time constants of precipitation scavenging are estimated from the fitting lines. Assuming that the precipitation rate during transportation is 1 $mm \cdot h^{-1}$, value of cumulative precipitation amount (mm) is inferred to correspond with the duration of precipitation (h). Consequently, the e-folding time of $N_{9–100}$ and $N_{100–300}$ can be estimated from the decay constant (pre-x coefficient) obtained using the exponential fitting lines in Fig. 3-7. The fitting lines in Fig. 3-7 suggest e-folding times at around 20 h for $N_{9–100}$ and 5 h for $N_{100–300}$. For below-cloud scavenging process, the e-folding time of particle concentration in sizes of 0.01 μm < D_p < 1 μm was estimated at the order of hundreds of hours for a small precipitation rate (1–10 $mm \cdot h^{-1}$) [*Sparmacher et al.,* 1993; *Andronache,* 2003]. Consequently, these results indicate that below-cloud scavenging is too slow to explain the observed decrease in particle concentrations with the increasing cumulative precipitation amount. In the case of in-cloud scavenging, the e-folding time of accumulation-mode concentration was estimated at the order of hours for small precipitation rate (1–10 $nm \cdot h^{-1}$) [*Scott,* 1982; *Andronache,* 2004]. This value agrees well with the e-folding time estimated for $N_{100–300}$ in this study. Therefore, the decrease in concentration of accumulation mode particles with the increasing cumulative precipitation amount is explainable mostly by in-cloud particle scavenging processes.

Figure 3-8 shows scatter plots of (a) $N_{9–100}$ and (b) $N_{100–300}$ versus the local precipitation

rate. Different from Fig. 3-7, a relation of particle concentration to the local precipitation rate is not apparent in Fig. 3-8. The local precipitation rate in Fig. 3-8 is dominated by small values less than 1 mm·h^{-1}, which possibly causes the lack of correlation between particle concentration and local precipitation rate in Fig. 3-8. However, high $N_{100–300}$ (> 100 cm^{-3}) was rarely observed under a higher local precipitation rate (> 0.1 mm·h^{-1}; Fig. 3-8b). Fog is usually associated with local precipitation at the site. Therefore, nucleation scavenging might engender lower $N_{100–300}$ rather than the scavenging process by raindrops of local precipitation. On the other hand, high $N_{9–100}$ (> 100 cm^{-3}) values were observed for higher local precipitation rate (> 0.1 mm·h^{-1}; Fig. 3-8a). Because unrealistically high supersaturation is required for activation of Aitken mode particles, nucleation scavenging under fog condition might not reduce $N_{9–100}$.

3.5. Relationship between particle number-size distribution and air-mass transportation with and without precipitation

Because of the effect on precipitation scavenging, the size distribution data set used in this study will be summarized by dividing the degree of precipitation scavenging and transportation pathways. Statistical information of size distributions representative for different air-mass transportation pathways with and without the effects of precipitation scavenging are shown in this section.

The type A air mass transported from over the Pacific Ocean was divided into two subgroups according to its cumulative precipitation amount: the first subgroup (type A-1) was defined as having cumulative precipitation of less than 5 mm; the second subgroup (type A-2) was defined as having cumulative precipitation amounts greater then 5 mm. The criterion of 5 mm of cumulative precipitation was set on the basis of the decay constant of $N_{100–300}$ estimated in Section 3-4. Local precipitation was rarely observed in type A. Therefore, local

precipitation will not be considered for type A. In contrast, type B, which was transported mainly from continental Asia, was divided into two subgroups according to local precipitation rate: the first subgroup (type B-1) was defined as having a local precipitation rate lower than the detection limit (0.1 $mm \cdot h^{-1}$); the second subgroup (type B-2) was defined as having a local precipitation rate higher than 0.1 $mm \cdot h^{-1}$. Cumulative precipitation amounts in type B were rarely greater than 5 mm. Therefore, the effect of the cumulative precipitation amount will not be considered for type B. Table 3-1 shows classifications based on the air-mass transportation pathway, cumulative precipitation amount, and the local precipitation rate. The numbers of hourly data of each subtype are also presented in Table 3-1.

Table 3-2 portrays data for modal parameters obtained using log-normal fitting on individual hourly size distributions and frequency of occurrence (FO) of each mode. Regarding the nucleation mode, because log-normal parameters of nucleation mode did not change with the air mass types and because the nucleation-mode FO was much lower (14% of entire data) than that of either the Aitken or accumulation mode, log-normal parameters of the nucleation mode are provided for all data in Table 3-2.

Figure 3-9 shows median particle number-size distributions of air mass types (a) A-1, (b) B-1, (c) A-2, and (d) B-2. The number-size distributions in Fig. 3-9 were calculated using the median of particle number density ($dN/d\log D_p$) of each size bin with resolution of 16 bins per decade. Note that the median number-size distributions shown in Fig. 3-9 were not reproduced from size distributions of median log-normal parameters in Table 3-2.

Types A-1 and B-1 are presumed to be less affected by precipitation and nucleation scavenging. For the accumulation mode, particle concentrations of types A-1 and B-1 were mutually similar (type A-1, 350 cm^{-3}; type B-1, 400 cm^{-3}) (see Table 3-2). However, Aitken mode concentrations were quite different between types A-1 (890 cm^{-3}) and B-1 (230 cm^{-3}). The FO of the Aitken mode was also different for types A-1 (100%) and B-1 (59%). As shown

in Figs. 3-9a and 3-9b, the maximum concentration of the median size distribution was found to be about 50 nm for type A-1 but much larger (>100 nm) for type B-1. The contrast in the particle size distribution between marine and continental air masses differs entirely from what was observed in the boundary layer. Statistical investigations of particle size distributions observed in the boundary layer in Germany [*Birmili et al.,* 2001] and in northern Europe [*Tunved et al.,* 2005] indicated that continental air masses have greater accumulation and Aitken mode concentrations, on average, than marine air masses.

A high particle-number concentration ($N_{9–300}$, 1200 cm^{-3}) dominated by Aitken mode particles (890 cm^{-3}) is an interesting characteristic of type A-1. Backward trajectories of type A-1 indicate that most type A-1 air masses subsided from the altitude of 4–5 km for the preceding 5 days (Fig. 3-2a). In addition to 5-day backward trajectories, I calculated 10-day backward trajectories for type A-1 air masses (Fig.3-10). The 10-day backward trajectories indicate that type A-1 air masses originated from altitudes of 5–10 km above the tropical Pacific Ocean during the preceding 10 days.

In the upper troposphere (8–12 km) over the tropical Pacific Ocean, high concentrations (5000–20000 cm^{-3} STP) of newly formed aerosol particles with $D_p < 10$ nm were observed frequently [*Clarke and Kapustin,* 2002]. Evolution of the number-size distribution of aerosol particles during subsidence from tropical upper troposphere to the subtropical lower troposphere was investigated using aerosol dynamic models [*Clarke,* 1993; *Raes,* 1995; *Raes et al.,* 2000]. According to the model studies during subsidence for 1–2 weeks from the upper troposphere, the aerosol particle concentration might decrease to 1000–2000 cm^{-3} by coagulation and its mode diameter of less than 10 nm might grow into Aitken-mode range through coagulation and condensation of gas-phase sulfuric acid. The total particle concentration and peak diameters of the dominant mode (40–60 nm) predicted by the model studies agree with type A-1 in this study. The models typically predict a mono-modal

distribution, but the size distribution of type A-1 was bimodal distribution with Aitken and accumulation modes (Fig. 3-9a). In the upper troposphere, concentrations of accumulation mode particles were reported to be very low (< ca. 10 cm^{-3}, STP) [e.g., *Clarke et al.,* 1999; *de Reus et al.,* 2001; *Zaizen et al.,* 2004]. The manner in which accumulation mode particles are added to the Aitken mode particles during subsidence from the tropical upper troposphere remains enigmatic. However, the following processes are considered to contribute to formation of the bimodal size distribution.

First, in-cloud sulfate production might add aerosol particles of accumulation-mode size through so-called cloud processes [*Hoppel et al.,* 1986; *Hoppel et al.,* 1994a, 1994b]. However, cloud formation is not realistic in a subsiding air mass. In fact, according to meteorological data (objective analysis data) along backward trajectories, relative humidities (RHs) of type A-1 are mostly lower than 60% (average RH, 55%) during transportation for the preceding 5 days, suggesting that cloud processes play a minor role in adding the accumulation mode particles. Next, the mixing process with an air mass that is rich in accumulation mode particles might add accumulation mode particles to the subsiding air mass under the mono-modal Aitken mode particles. According to meteorological data along backward trajectories of type A-1 masses, water mixing ratios in type A-1 masses show a gradual increase from 3 $g \cdot kg^{-1}$ to 6 $g \cdot kg^{-1}$ during transportation for the preceding 5 days, suggesting gradual mixing of subsiding air with low-altitude air containing water vapor and accumulation mode particles during transportation. This process might not cause a great decrease of Aitken-mode concentration because gradual dilution of Aitken-mode particles leads to a slow decrease of Aitken-mode concentration through coagulation if Aitken mode particles originated in the upper troposphere were diluted through gradual mixing with low-altitude air during subsidence.

In type B-1, mono-modal size distributions account for 46% of the entire distribution.

Most (80%) of the mono-modal size distribution is of mono-modal accumulation mode with large average σ_g (ca. 1.7; Table 3-2). Mono-modal accumulation modes were observed frequently, especially during July 29 – August 5 (Fig. 3-6), when warm humid air masses (Fig. 3-3a) were transported from over the coastal area of the Yellow Sea in China (Fig. 3-5a). The coastal area of the Yellow Sea is a highly industrialized, major source of air pollutants in Asia [*Streets et al.,* 2003].

To our knowledge, in industrialized areas of China, measurement of particle number-size distributions of $D_p < 100$ nm has not been reported. However, in an extremely polluted Asian city, New Delhi, India, mono-modal accumulation modes with high particle concentration (order of 10^4 cm^{-3}) were observed during nighttime when the influence of primary particle emissions from traffic, biomass and refuse burning, and cooking are low [*Mönkkönen et al.,* 2005]. The particle size distributions in industrialized areas in China might resemble those of New Delhi. The mono-modal accumulation mode observed in type B-1 might be explained by air-mass transportation from the highly polluted area and dilution with clean air during transportation to Mt. Norikura. On the other hand, because mono-modal accumulation modes are observed frequently in humid air masses, the lack of Aitken mode in the size distributions might also be explained by impaction scavenging of Aitken-mode particles by cloud droplets in non-precipitation clouds (see below).

Regarding type A-2 masses, FO of accumulation mode and median concentration of accumulation mode particles were low (54%, 100 cm^{-3}). As described in Section 3-4, it is inferred that in-cloud scavenging mainly accounts for low accumulation-mode concentration in type A-2 air masses. The particles activated as cloud condensation nuclei will be removed by precipitation from clouds. That might engender the low FO of accumulation mode and low accumulation-mode concentration in type A-2 masses. On the other hand, Aitken-mode concentration was also low (100 cm^{-3}) in type A-2, although the FO of Aitken mode was high

(100%). Smaller particles, which are inactive as cloud condensation nuclei (D_p< ca. 0.1 μm), might not be removed by nucleation scavenging at the first stage of cloud formation. However, they might be removed via diffusion to the cloud droplets in the clouds. I estimate scavenging speed of cloud interstitial aerosol particles inside cloud by the Brownian diffusion to cloud droplets [*Fuchs,* 1964], assuming that the cloud droplets' diameter is 20 μm, the cloud droplet concentration is 50–500 cm^{-3} [*Pruppacher and Klett,* 1997, pp 15–24], the dry diameters of cloud interstitial particles are 50 nm (corresponding to peak diameter of the Aitken-mode of type A-2), and that the hygroscopic growth factor of interstitial particle diameter is 2.7 (growth factor of $(NH_4)_2SO_4$ particle at RH 98 % [*Tang and Munkelwitz,* 1994]). The e-folding time of a cloud interstitial aerosol particle concentration is estimated as about 10–100 h, which is consistent with the decay time estimated for $N_{9–100}$ in Section 3-4 (20 h). The low Aitken-mode concentration of the type A-2 air mass might be caused by scavenging through diffusion to cloud droplets.

In type B-2, the FO of accumulation mode and concentration of accumulation mode particles were low (38%, 100 cm^{-3}). The FO of the Aitken mode was high (ca. 100%) in type B-2, but unlike type A-2, the Aitken-mode concentration (340 cm^{-3}) was not so low as in type B-2. As mentioned above, the lack of accumulation mode particles in type B-2 masses might result mostly from nucleation scavenging in fog, which is usually associated with local precipitation at the site.

The results shown in this chapter suggest that the precipitation amount experienced by an air mass is an important factor determining the number concentration and shape of the size distribution of sub-micrometer particles. Importance of precipitation scavenging process as a controlling factor for number-size distribution of aerosol particles was pointed out also in the boundary layer by *Tunved et al.* [2004] on the basis of statistical analyses using meteorological data along backward trajectories of air masses. Statistical information of

number-size distributions of aerosol particles combined with the degree of precipitation scavenging would be useful for model verification of various models that address or incorporate aerosol parameters. However, to our knowledge, no such a study has provided statistical information of size distribution parameters with the degree of precipitation scavenging experienced by air mass. A long-term observation of number-size distribution of free tropospheric aerosol particles has been performed at Jungfraujoch in the Swiss Alps (3580 m a.s.l.) [*Weingartner et al.,* 1999]. Without data classification according to cumulative precipitation amounts, as used in this study, meaningful aerosol parameters might not be obtained.

3.6. Chapter summary

Number-size distributions of free tropospheric aerosol particles at Mt. Norikura were analyzed in terms of their relation with the air mass transportation pathway and meteorological parameters, especially for cumulative precipitation amount in air mass for the preceding 24 h before arrival and local precipitation rate.

Aerosol particle concentrations in accumulation-mode range ($N_{100–300}$) were decreased by an order of magnitude when the cumulative precipitation amount increased from 0 mm to 20 mm. The cumulative precipitation amount prior to arrival at the observation site was suggested an important factor that considerably decreased the number concentration of accumulation mode particles. In the case of local precipitation with fog at the site, low $N_{100–300}$ was also observed, possibly because of nucleation scavenging by local fog droplets.

Air masses observed during the observation were classified into two air-mass types transported from over the Pacific Ocean and continental Asia. Considering air masses without precipitation before arrival, accumulation-mode concentration was almost the same in air masses transported from over continental Asia (400 cm^{-3}) and the Pacific Ocean (350 cm^{-3}).

Aitken-mode concentrations were high (890 cm^{-3}) in the air mass that arrived from over the subtropical Pacific Ocean, but lower in the air mass that had been transported from continental Asia (230 cm^{-3}). Backward trajectories suggest that air masses with high Aitken-mode concentration mainly originated from the tropical upper troposphere.

4. Occurrence of nucleation mode particles: Favorable conditions for new particle formation

In this chapter, nucleation mode is defined as a mode that first appears in the size range below 20-nm diameter and which is observed continuously for several hours. Occurrence of nucleation mode suggests new particle formation event occurred recently in the air mass. To find favorable factor for new particle formation event, this chapter focuses on the relation of occurrence of nucleation mode particles with diurnal variation of the local wind system (down-slope mountain and up-slope valley winds).

Section 4-1 describes selection of sunny days during which clear diurnal variation of the local wind system likely occurs at the observation site to ensure proper analysis were selected. Nucleation mode particles were observed during four sunny days; the four sunny days are referred to as new particle formation (NPF) event days in this study. Section 4-2 describes diurnal variation of number-size distribution of aerosol particles in the relation with local meteorological conditions during an NPF event. In Section 4-3, to evaluate the importance of pre-existing particle concentration (condensation sink) and inorganic precursor gas (SO_2 and NH_3) concentrations as controlling factors for the NPF events at Mt. Norikura, those parameters in the local wind system are compared between the NPF event days and non-event sunny days.

4.1. Selection of sunny day

To ensure proper analysis of aerosol data in terms of their relationship with diurnal variation of the local wind system, I selected sunny days during which clear diurnal variation of the local wind system is likely to occur at the observation site. For this study, a sunny day is defined as a day during which the amount of global solar radiation during 5–12 h LT (UT plus 9 h) was greater than 10 $MJ \cdot m^{-2}$ at the observatory. Visual sky observation during

intensive observation periods confirmed that the weather condition was sunny or clear on those days. During the observation periods, 23 sunny days were identified. Figure 4-1 shows (a) the temporal variation of hourly local air temperature and its 24-h moving average at the observation site and (b) the deviations of the hourly temperature from the 24-h moving average (ΔT), which represents the diurnal component of the temperature variation mainly caused by radiative cooling and solar heating of the mountain surface. Circles in row b of Fig. 4-1 signify the sunny days based on the solar radiation amount. The amplitude of diurnal variation of air temperature was large on the sunny days. For that reason, clear diurnal variation of down-slope and up-slope winds likely emerged on those days.

Among the 23 sunny days, a distinct nucleation mode was observed on four days: 22 September 2001, 21 August 2002, 18 September 2002, and 24 September 2002. Those days are defined as NPF event days in this study. Star marks in Fig. 4-1b indicate the four NPF event days.

4.2. Occurrence of nucleation mode particles in up-slope valley winds

As an example, Fig. 4-2a shows the diurnal evolution of the particle size distribution on an NPF event day (22 September 2001). Figure 4-2b shows growth of the nucleation mode diameter on the day. The nucleation mode appeared at around noon and ceased at around 19 h LT. The nucleation mode particle diameter increased from 13 nm to about 30 nm almost linearly with time. From the slope of the fitting line in Fig. 4-2b, the growth rate of nucleation mode particles was estimated as 2.6 $nm \cdot h^{-1}$. Figure 4-2c shows diurnal variations of global solar radiation, the water vapor mixing ratio (w), and the total number concentration of particles with 9–60-nm diameter ($N_{9–60}$). The size range of 9–60-nm was set to exclude accumulation mode particles from $N_{9–60}$. In fact, $N_{9–60}$ is almost the same as the total number concentration of nucleation mode particles. $N_{9–60}$ increased from about 150 cm^{-3} to 600 cm^{-3} at

around noon and decreased to about 50 cm^{-3} after sunset. Temporal variation of $N_{9–60}$ closely resembled that of w, even the short-term fluctuation at around 15 h LT. The close relation between $N_{9–60}$ and w suggests that nucleation mode particles were transported to the observatory along with humid air. Figure 4-3d shows the diurnal variation of CS and SO_2 and NH_3 concentrations. Both CS and the NH_3 concentration increased from the morning to afternoon. During that time, SO_2 showed a consistently low concentration of about 0.02 ppbv.

Figure 4-3 shows hourly particle size distributions from 11 h to 13 h LT of 22 September 2001. At the beginning of the event, the nucleation mode first appeared at 13 nm diameter at 12 h LT at the observation site. Assuming that nucleation mode particles observed after 12 h LT were formed by nucleation and subsequent growth of the nucleated particles at the rate of few nanometers per hour in-situ at the site, the particle size distribution with increasing particle concentration toward a smaller detection size limit would be expected before 12 h LT. However, such a size distribution was not observed before 12 h LT; particles having mode diameter at 13 nm appeared suddenly at 12 h LT on an hourly basis. The evolution of the size distribution shape suggests that the observed nucleation mode particles were not formed in situ at the site, but were formed at a distant location, then transported to the site.

Figure 4-4 shows vertical profiles of RH, the water vapor mixing ratio (w), the air temperature (T), and the potential temperature (θ) based on aerological data at Wajima at 9 h LT of 22 September 2001. Aerological data show a distinctive boundary at about 2200 m a.s.l., indicating a well mixed layer with uniform θ and high w (ca. 5 $g \cdot kg^{-1}$) below the temperature inversion. The water vapor mixing ratio decreased sharply to about 1 $g \cdot kg^{-1}$at the top of the mixed layer; this is consistent with w observed at the observatory in the morning (Fig. 4-2c). On the other hand, humid air was observed at the observatory in the afternoon because of up-slope valley winds carrying humid air from the mixed layer to the observatory (Fig. 4-2c).

Based on the correlation between $N_{9–60}$ and w (Fig. 4-2c) and the vertical distribution of w (Fig. 4-4), it is inferred that nucleation mode particles were formed in the air transported from the mixed layer air but not in the air transported from the free troposphere. Although *CS* in the mixed layer air was larger than that in the free tropospheric air (Fig. 4-2d), nucleation mode particles appeared in up-slope air from the mixed layer. This appearance suggests that the source rate of condensable vapors is high in the mixed layer air, exceeding the prohibiting effects of *CS* on NPF.

Similar to the example presented above, nucleation mode particles were observed in up-slope valley winds on other NPF event days. The growth rate of nucleation mode particles of 3.1 $nm \cdot h^{-1}$, which resembles the growth rate of 22 September 2001 (2.6 $nm \cdot h^{-1}$), was observed on another NPF event day (21 August 2002). For other NPF event days (18 and 24 September 2002), I can not determine the growth rate of nucleation mode particles either because the nucleation mode showed no definite mono-modal shape or because continuous observation was obstructed by local air contamination. The particle growth rates estimated for the two NPF event days (2.6–3.1 $nm \cdot h^{-1}$) suggest condensable vapor concentrations C_v of (2–3) $\times 10^7$ $molecules \cdot cm^{-3}$ and its source rates Q of $10^{4–5}$ $molecules \cdot s^{-1}\ cm^{-3}$, based on the analysis described in Section 2–4.

Increases of freshly formed particle concentrations in the air of up-slope valley wind have been observed also at other mountain sites: Mauna Loa, Hawaii (3400 m a.s.l.) [*Weber et al.,* 1995], Canary Islands (2360 m a.s.l.) [*Raes et al.,* 1997], Jungfraujoch, Swiss (3580 m a.s.l.) [*Weingartner et al.,* 1999], and Mt. Lemmon, Arizona (2790 m a.s.l.) [*Shaw,* 2007]. Growth rates of nucleation mode particles 3–4.5 $nm \cdot h^{-1}$ and 10–23 $nm \cdot h^{-1}$ were reported at Jungfraujoch and Mt. Lemmon, respectively. The former is similar to the result of this study (2.6–3.1 $nm \cdot h^{-1}$) but the latter is much larger than that, although the growth rates reported at Jungfraujoch and Mt. Lemmon might not be directly comparable to the result of this study

because the methods for determining the growth rate was different between them.

To investigate transportation pathways of the air-masses observed on the four NPF event days, backward trajectories of the air-masses were calculated. Figure 4-5 shows three-day backward trajectories calculated from an altitude in the mixed layer (600 m a.s.l.) near Mt. Norikura at 9 h LT of the NPF event days. The trajectories indicate that air-masses of the NPF event days were transported from over the Sea of Japan. However, the air-masses in the mixed layer were transported over land for 7–12 hours before arrival at Mt. Norikura. Assuming onset of nucleation after sunrise of the event days, NPF events might occur over land, and precursor gases emitted from ground surface might participate in that.

4.3. Comparison of *CS*, SO_2 and NH_3 concentrations between NPF event and non-event sunny days

In this section, *CS*, and SO_2 and NH_3 concentrations in the mixed layer air condition are compared for NPF event days and non-event sunny days.

The time windows for the mixed layer conditions were set to 12–16 h LT. Figure 4-6a shows the day-to-day variation of average *CS* in the time window for sunny days only. Star marks at the top of Fig. 4-6a indicate NPF event days. The value of *CS* on NPF event days was lower than that on the non-event days on average. The average *CS* on NPF event days was about 50% of that on non-event days (Table 4-1). NPF event days are characterized by low *CS* values, suggesting that low *CS* in the mixed layer is important for initiating an NPF event at Mt. Norikura.

Figure 4-6b shows SO_2 concentrations in the afternoon on sunny days. Figure 4-6c shows NH_3 concentrations based on the acid-impregnated filter samples obtained within 10–17 h LT of the sunny days. The SO_2 and NH_3 concentrations showed no systematic correlation with NPF events. Gas-phase H_2SO_4 is produced through photochemical reaction of

SO_2 in the atmosphere [*Finlayson-Pitts and Pitts,* 2000]. Therefore, if H_2SO_4 or NH_3 were major precursors for initiating homogeneous nucleation and subsequent particle growth, high SO_2 or NH_3 concentration would be a favorable condition for an NPF event. However, this study found no positive correlation between an NPF event and SO_2 or NH_3 concentrations (Table 4-1).

Results of the previous chapter suggest that precipitation scavenging during air-mass transportation is an important factor causing significant decrease in pre-existing particle concentration. In addition, *Osada et al.* [2007] suggest that advection of clean air descending from a higher altitude is also a factor causing low pre-existing particle concentrations. The air-mass backward trajectories (Fig. 4-5) indicate that air-masses of the mixed layer traveled below 1500 m a.s.l. Furthermore, I examined precipitation amounts during air-mass transportation according to objective analysis data along the trajectories. The precipitation amounts along the air-mass trajectories of the NPF event days were almost zero for more than three days before arrival. Those facts suggest that low *CS* in the mixed layer air on the NPF event days was not caused by advection of clean air originated from higher altitude or precipitation scavenging.

Figure 4-7 shows weather maps (geopotential height and temperature fields at 850 hPa surface and the location of fronts at the surface) of the NPF event days. On all of the event days, the observation site was located behind a cyclone followed by a cold front and covered by colder air advected from the north. In three cases from the four NPF events, the cyclones were tropical cyclones (typhoons) that approached from the south and passed northeastward by the east coast of Japan's main island. Associated with the meteorological situation, the NPF events in this study always coincided with lower temperatures (see the variation of the 24-h moving average of air temperature in Fig. 4-1a). Horizontal advection of cold air from the northern high latitudes might bring a clean air mass with low *CS* in the mixed layer and

trigger NPF events at Mt. Norikura. In fact, concentrations of SO_4^{2-}, a major ionic component of atmospheric aerosol, in the Arctic lower troposphere are very low (approximately 0.1 $\mu g \cdot m^{-3}$ [*Sirois and Barrie,* 1999]) in summer – early autumn compared to the concentrations (>2 $\mu g \cdot m^{-3}$) normally observed at remote sites in Japan [e.g., *Mukai et al.,* 1990; *Osada et al.,* 2007].

Some relations among NPF events, synoptic-scale meteorology, and air-flow patterns have been found also in northern Europe [e.g., *Nilsson et al.,* 2001b; *Vana et al.,* 2004], Italy [*Sogacheva et al.,* 2007], and China [*Wu et al.,* 2007]. In northern Europe, similar to our results, a strong connection between the NPF event and cold air advection was reported; low *CS* was identified as an important factor for the NPF event [e.g. *Nilsson and Kulmala,* 2006].

4.4. Chapter summary

In up-slope valley wind condition in the daytime on sunny days, nucleation mode was observed below 20 nm in diameter on four days (NPF event days). Clear correlation between nucleation mode particle concentrations and the water vapor mixing ratio during the NPF event days suggests that nucleation mode particles were formed in the air transported from the mixed layer, but not in the free tropospheric air. Because *CS* was consistently higher in the mixed layer air than in the free tropospheric air, the source rate of condensable vapors in the mixed layer air must be higher than that in the free tropospheric air, overcoming the inhibitory effects on NPF, which are attributable to high *CS* in the mixed layer air. Growth rates of nucleation mode particles during the NPF events were 2.6–3.1 $nm \cdot h^{-1}$, suggesting that condensable vapor concentration and its source rate in the mixed layer were of approximately 10^7 molecules$\cdot cm^{-3}$ and $10^{4–5}$ molecules$\cdot s^{-1}$ cm^{-3}, respectively.

The *CS* on NPF event days was significantly lower than that on non-event sunny days in the mixed layer air on average. However, no positive correlation was found between NPF

events and SO_2 or NH_3 concentrations.

Based on the meteorological data along backward trajectories of air masses, the low *CS* on the NPF event days was not caused by recent precipitation scavenging before arrival. On the NPF event days, the observation site was covered in all cases by cold air advected from the north. Advection of the cold air mass might bring low *CS* within the mixed layer and trigger an NPF event at Mt. Norikura. Aerosol concentrations in summer Arctic air are expected to be quite low. Therefore, advection of the northern cold air mass might decrease *CS* in the mixed layer at Mt. Norikura.

5. Factors controlling variation of the number-size distribution of submicron aerosol particles in the atmosphere

Several types of number-size distribution of submicron aerosol particles were observed at Mt. Norikura, and discussions in the previous chapters were focused on factors controlling variation of the size distributions. The atmospheric observation performed in this study is not a perfect Lagrangian experiment, but the results of the observation shows advection of various air masses that experienced different processing over different time scales during transportation. Thus, the knowledge about factors controlling variation of particle number-size distribution at Mt. Norikura might provide information on how characteristics of number-size distribution of aerosol particles are connected to formation, growth, and removal processes of aerosol particles in a Lagrangian perspective.

Figure 5-1 shows a schematic diagram of envisaged evolution of number-size distribution of submicron aerosol particles in relation with particle formation, growth, and removal processes. Stage-1 in Fig. 5-1 is the distribution showing high nucleation mode particle concentration, which results from new particle formation process through homogenous nucleation, as seen in Fig. 4-3 in this study. Stage-1 will proceeds stage-2 through particle growth processes by condensation of low-volatile vapors and self-coagulation. Stage-2 is characterized by high Aitken mode particle concentration, which corresponds to the size distribution observed in the air-mass transported from the tropical upper-troposphere without precipitation in this study (type A-1 in Fig. 3-9a). Stage-3 is characterized by the dominant accumulation mode particle concentration, which corresponds to the size distribution observed in the air-mass transported from over continental Asia without precipitation (type B-1 in Fig. 3-9b). According to the general aerosol dynamics governing temporal evolution of size distribution of aerosol particles, stage-2 and stage-3 will be connected by aging process of Aitken mode particles (e.g., cloud processing and condensation

etc.), although the processes relating to the change from stage-2 to stage-3 were not directly discussed in this study. Accumulation mode particles, which often act as cloud condensation nuclei, might be formed through such aging processes. Stage-4 is the terminal stage that formed after precipitation scavenging (mainly in-cloud scavenging), which corresponds to the number-size distribution observed in the air mass with high cumulative precipitation amounts (type A-2 in Fig. 3-9c).

This study demonstrated that precipitation scavenging, especially in-cloud scavenging, decreases both of Aiken and accumulation mode particle concentrations effectively. In addition, favorable conditions for new particle formation event were investigated; advection of clean air-mass with low pre-existing particle concentration was found to be a favorable factor initiating new particle formation event at Mt. Norikura. Theses results suggest that precipitation scavenging provides favorable condition for new particle formation by decreasing pre-existing particle concentration, although new precursor vapors must be added after precipitation scavenging to initiate new particle formation. Based on these results, stage-1 might be connected to stage-4 in a cycle of number-size distribution of aerosol particles as shown Figure 5-1. Precipitation scavenging might be a key process driving the cycle of number-size distribution of aerosol particles in the atmosphere.

6. Summary and Conclusions

Number-size distributions of atmospheric aerosol particles of 9–300-nm diameters were observed during September 2001 and August–September 2002 (48 days in all) at Mt. Norikura. First, number-size distributions of free tropospheric aerosol particles, which were observed in down-slope wind condition during the nighttime, were analyzed in terms of their relation to the air-mass transportation pathways and cumulative precipitation amount during air-mass transportation. Next, this study investigated atmospheric conditions favorable for occurring nucleation mode particles, which indicates new particle formation through homogenous nucleation and subsequent particle growth occurs during atmospheric transport immediately before arrival at the observation site.

In free tropospheric condition during the nighttime, accumulation and Aitken modes were dominant over nucleation mode in both frequency of occurrence and modal concentration, and nucleation mode with geometric mean diameter below 20 nm was not observed. To investigate effects of the air-mass transportation pathways and precipitation scavenging during air-mass transportation on number-size distribution of aerosol particles, size distributions observed in the free tropospheric condition were compared with cumulative precipitation amounts experienced by the air masses during transportation and air-mass backward trajectories. When the cumulative precipitation amount for the preceding 24 h before arrival increased from 0 to 20 mm, particle concentrations in accumulation mode range (100–300 nm diameters) were decreased by an order of magnitude, and Aitken mode range (9–100 nm diameters) were decreased by about half. The cumulative precipitation amount prior to arrival at the observation site was suggested as a important factor that decrease the number concentration of Aitken and accumulation mode particles. The time constant of precipitation scavenging estimated from the relationship between the cumulative precipitation and particle concentration suggests that the particle decrease caused by mostly by in-cloud

scavenging process.

Considering air-masses without precipitation before arrival, concentration of accumulation mode particles was almost the same in the air-masses transported from over the continental Asia (400 cm^{-3}) and the Pacific Ocean (350 cm^{-3}). Aitken mode concentrations were high (890 cm^{-3}) in the air mass that arrived from over the subtropical Pacific Ocean, but lower in the air mass that had been transported from over continental Asia (230 cm^{-3}). Air-mass transportation pathway was found to be an important factor for Aitken mode particle concentration in free tropospheric aerosol at Mt. Norikura.

Nucleation mode were observed in the diameter range below 20 nm during daytime on four days (NPF (new particle formation) event days) of 23 sunny days that showed clear diurnal variation of down-slope mountain and up-slope valley winds. The clear correlation between nucleation mode particle concentrations and water vapor mixing ratio suggests that nucleation mode particles were formed in the mixed layer air transported by the up-slope valley wind. Because pre-existing particle (Aitken and accumulation mode particle) concentrations were consistently higher in the mixed layer air than in the free tropospheric air, the source rate of condensable vapors in the mixed layer must be higher than that in the free tropospheric air, overcoming the inhibitory effects on new particle formation, which are attributable to high pre-existing particle concentration in the mixed layer air.

Pre-existing particle concentration in the mixed layer air on the NPF event days were significantly lower than that on the non-event sunny days. However, no positive correlation was found between NPF events and SO_2 or NH_3 concentrations. Advection of clean air mass with low pre-existing particle concentration within the mixed layer might trigger NPF event at Mt. Norikura.

Based on the variation of number-size distributions of aerosol particles observed at Mt. Norikura and factors controlling the size distributions discussed in this study, a conceptual

scheme of a cycle of number-size distribution of atmospheric aerosol particles, relating to particle formation, growth, and removal processes is suggested in a Lagrangian perspective. Precipitation scavenging might be a key process for driving the cycle of number-size distribution of aerosol particles in the atmosphere.

Acknowledgements

I am grateful to Dr. K. Osada for valuable guidance and continuous encouragements. I am also grateful to Prof. Y. Iwasaka for providing me with the opportunity to study the atmospheric aerosol and the use of SMPS. I would like to thank Dr. M. Kido for helping with aerosol sampling at Mt. Norikura and warm encouragements. I would like to thank Prof. T. Shibata, and Dr. K. Matsunaga for many discussions and useful suggestions.

I am grateful for the great support and help of the staff of the Norikura Observatory of ICRR, University Tokyo. I am also grateful to the members participated in the aerosol observation at Mt. Norikura: Drs. Y. Inomata and A. Matsuki, and Messrs. T. Nezuka, Y. Inomiya, and T. Ohtsubo. I wish to thank many colleagues at Solar-Terrestrial Environment Laboratory and Graduate School of Environmental Studies, Nagoya University.

References

Anderson, T. L., R. J. Charlson, D. M. Winker, J. A. Ogren, K. Holmén (2003), Mesoscale variations of tropospheric aerosols, *J. Atmos. Sci.*, 60, 119–136.

Andres, R. J. and A. D. Kasgnoc (1998), A time-averaged inventory of subaerial volcanic sulfur emissions, *J. Geophys. Res., 103,* 25251–25261.

Andronache, C. (2003), Estimated variability of below-cloud aerosol removal by rainfall for observed aerosol size distributions. *Atmos. Chem. Phys., 3*, 131–143.

Andronache, C. (2004), Estimates of sulfate aerosol wet scavenging coefficient for locations in the Eastern United States, *Atmos. Environ.*, *38*, 795–804.

Anttila, T., H. Vehkamäki, I. Napari, and M. Kulmala (2005), Effect of ammonium bisulphate formation on atmospheric water-sulphuric acid-ammonia nucleation, *Boreal. Environ. Res.*, *10*, 511–523.

Ball, S. M., D. R. Hanson, F. L. Eisele, and P. H. McMurry (1999), Laboratory studies of particle nucleation: Initial results for H_2SO_4, H_2O, and NH_3 vapors, *J. Geophys. Res.*, *104*, 23709–23718.

Barry, R. G. (1992), *Mountain Weather and Climate* -2nd edition, Routledge, New York.

Berndt, T., O. Böge, F. Stratmann, J. Heintzenberg, M. Kulmala (2005), Rapid formation of sulfuric acid particles at near-Atmospheric conditions, *Science, 307,* 698–700.

Birmili, W. and A. Wiedensohler (2000), New particle formation in the continental boundary layer: Meteorological and gas phase parameter influence, *Geophys. Res. Lett., 27*, 3325–3328.

Birmili, W., A. Wiedensohler, J. Heintzenberg, and K. Lehmann (2001), Atmospheric particle number size distribution in central Europe: Statistical relations to air masses and meteorology, *J. Geophys. Res., 106*(D23), 32005–32018.

Birmili, W., H. Berresheim, C. Plass-Dülmer, T. Elste, S. Gilge, A. Wiedensohler, and U. Uhrner (2003), The Hohenpeissenberg aerosol formation experiment (HAFEX): a long-term study including size-resolved aerosol, H_2SO_4, OH, and monoterpenes measurements, *Atmos. Chem. Phys.*, *3*, 361–376.

Boy, M., M .Kulmala, T. M. Ruuskanen, M. Pihlatie, A. Reissell, P. P. Aalt, P. Keronen, M. Dal Maso, H. Hellen, H. Hakola, R. Jansson, M. Hanke, and F. Arnold (2005),

Sulphuric acid closure and contribution to nucleation to mode particle growth, *Atmos. Chem. Phys.*, *5*, 863–878, SRef-ID: 1680-7324/acp/2005-5-863.

Buzorius, G., Ü. Rannik, D. Nilsson, and M. Kulmala (2001), Vertical fluxes and micrometeorology during aerosol particle formation events, *Tellus*, *53B*, 394–405.

Charlson, R. J. and J. Heintzenberg (1995), *Aerosol Forcing of Climate*, John Wiley & Sons, New York.

Clarke, A. D. (1993), Atmospheric nuclei in the Pacific Midtroposphere: Their nature, concentration, and evolution, *J. Geophys. Res., 98,* 20633–20627.

Clarke, A. D., J. L. Varner, F. Eisele, R. L. Mauldin, D. Tanner, and M. Litchy (1998), Particle production in the remote marine atmosphere: Cloud outflow and subsidence during ACE 1, *J. Geophys. Res., 103,* 16397–16409.

Clarke, A. D., F. Eisele, V. N. Kapustin, K. Moore, D. Tanner, T. Mauldin, M. Litchy, B. Lienert, M. A. Carroll, and G. Albercook (1999), Nucleation in the equatorial free troposphere: Favorable environments during PEM-Tropics, *J. Geophys. Res., 104,* 5735–5744.

Clarke, A. D. and V. N. Kapustin (2002), A Pacific aerosol survey. Part I: A decade of data on particle production, transport, evolution, and mixing in the troposphere, *J. Atmos. Sci., 59,* 363–382.

de Reus, M., R. Krejci, J. Williams, H. Fischer, R. Scheele, and J. Ström (2001), Vertical and horizontal distributions of the aerosol number concentration and size distribution over the northern Indian Ocean, *J. Geophys. Res., 106,* 28629–28641.

Draxler, R. R. and G. D. Rolph (2003), HYSPLIT (HYbrid Single-Particle Lagrangian Integrated Trajectory) model access via NOAA ARL READY Website http://www.arl.noaa.gov/ready/hysplit4.html, NOAA Air Resources Laboratory, Silver Spring, MD.

Finlayson-Pitts, B. J., and J. N. Pitts, Jr. (2000), *Chemistry of the upper and lower atmosphere: Theory, experiments, and application*, Academic Press Inc., New York.

Fuchs, N. A. (1964), *The Mechanics of Aerosols*, pp. 288–302, Pergamon, New York.

Fuchs, N. A., and A. G. Sutugin (1971), High-dispersed aerosols, *Topics in current aerosol research*, G. M. Hidy and J. R. Brock, Pergamon, New York, pp1–60.

Greenfield, S. (1957), Rain scavenging of radioactive particulate matter from the atmosphere, *J. Meteor., 14*, 115–125.

Grover, S. N., H. R. Prupacher, and A. E. Hamielec (1977), A numerical determination of the efficiency with which scherical aerosol particles collide with Spherical water drops due to inertial impaction and phoretic and electrical forces, *J. Atmos. Sci., 34,* 1655–1663.

Hanson, D. R., and F. Eisele (2000), Diffusion of H_2SO_4 in humidified nitrogen: hydrated H_2SO_4, *J. Phys. Chem. A*, *104*, 1715–1719.

Held, A., A. Nowak, W. Birmili, A. Wiedensohler, R. Forkel, and O. Klemm (2004), Observations of particle formation and growth in a mountainous forest region in central Europe, *J. Geophys. Res.*, *109*, D23204, doi: 10.1029/2004JD005346.

Hinds, W. C. (1999), *Aerosol Technology: Properties, Behavior, and Measurement of Airborne Particles, Second Edition,* pp. 162–164, John Wiley & Sons, New York.

Holmes, N. S. (2007), A review of particle formation events and growth in the atmosphere in the various environments and discussion of mechanistic implications, *Atmos. Environ.*, *41*, 2183–2201.

Hoppel, W. A., G. M. Frick, and R. E. Larson (1986), Effect of nonprecipitating clouds on the aerosol size distribution in the marine boundary layer, *Geophys. Res. Lett., 13*, 125–128.

Hoppel, W. A., G. M. Frick, J. W. Fitzgerald, and R. E. Larson et al. (1994a), Marine boundary layer measurements of new particle formation and the effects nonprecipitating clouds have on aerosol size distribution, *J. Geophys. Res., D99*, 14443–14459.

Hoppel, W. A., G. M. Frick, and J. W. Fitzgerald (1994b), A cloud chamber study of the effect that nonprecipitating water clouds have on the aerosol size distribution, *Aerosol Sci. and Technol*., *20*, 1–30.

International Critical Tables of Numerical Data, Physics, Chemistry and Technology (1928), McGraw-Hill, New York, Vol. III, 43–45.

Junge, C. (1955), The size distribution and aging of natural aerosols as determined from electrical and optical data on the atmosphere, *J. Meteor., 12,* 13–25.

Kajino, M., H. Ueda, and H. Satsumabayashi, J. An (2004), Impacts of the eruption of Miyakejima Volcano on air quality over far east Asia, *J. Geophys. Res., 109,* D21204, doi:10.1029/2004 JD004762.

Keil A., and M. Weidenhoser (2001), Bursts of Aitken mode and ultrafine particles observed at the top of continental boundary layer clouds, *J. Aerosol Sci.*, *32*, 649–660.

Kerminen, V.-M., L. Pirjola, and M. Kulmala (2001), How significantly does coagulational scavenging limit atmospheric particle production? *J. Geophys. Res.*, 106, 24119–24125.

Kerminen, V.-M., H. Lihavainen, M. Komppula, Y. Viisanen, and M. Kulmala (2005), Direct observational evidence linking atmospheric aerosol formation and cloud droplet activation, *Geophys. Res. Lett.*, *32*, L14803, doi:10.1029/2005GL023130.

Kido, M., K. Osada, K. Matsunaga, and Y. Iwasaka (2001), Diurnal variation of ionic aeorosol species and water-soluble gas concentrations at a high-elevation site in the Japanese Alps, *J. Geophys. Res.*, *106*, 17335–17345.

Kido, M. (2001), Temporal variation of ionic concentrations in aerosol particles and water-soluble gas concentrations from early winter to spring at Mt. Tateyama: The origin, transform process and chemical composition of free tropospheric sulfate over Japan, PhD thesis, pp 13–16, Nagoya University, Nagoya, Japan.

Korhonen, P, M. Kulmala, A. Laaksonen, Y. Viisanen, R. McGraw, and J. H. Seinfeld (1999), Ternary nucleation of H_2SO_4, NH_3, and H_2O in the atmosphere, *J. Geophys. Res.*, *104*, 26349–26353.

Kulmala, M., A. Laaksonen, and L. Pirjola (1998), Parameterizations for sulfuric acid/water nucleation rates, *J. Geophys. Res.*, *103*, 8301–8307.

Kulmala, M., L. Pirjola, and J. M. Mäkelä (2000), Stable sulphate clusters as a source of new atmospheric particles, *Nature, 404,* 66–69.

Kulmala, M., M. Dal Maso, J. M. Mäkelä, L. Pirjola, M. Väkevä, P. Aalto, P. Miikkulainen, K. Hämeri, and C. D. O'Dowd (2001), On the formation, growth and composition of nucleation mode particles, *Tellus*, *53B*, 479–490.

Kulmala, M., H. Vehkamäki, T. Petäjä, M. Dal Maso, A. Lauri, V.-M. Kerminen, W. Birmili, and P. H. McMurry (2004), Formation and growth rates of ultrafine atmospheric particles: a review of observations, *J. Aerosol Sci.*, 35, 143–176.

Lee, L. W., and H. Chen (1984), Coagulation rate of polydisperse particles, *Aerosol Sci. and Technol., 3,* 327–334.

Lee, S. -H., J. M. Reeves, J. C. Wilson, D. E. Hunton, A. A. Viggiano, T. M. Miller, J. O.

Ballenthin, L. R. Lait (2003), Particle formation by ion nucleation in the upper troposphere and lower stratosphere, *Science, 301,* 1886–1889.

Lihavainen, H., V.-M. Kerminen, M. Komppula, J. Hatakka, V. Aaltonen, M. Kulmala, and Y. Viisanen (2003), Production of "potential" cloud condensation nuclei associated with atmospheric new-particle formation in northern Finland, *J. Geophys. Res.*, *108*, 4782, doi:10.1029/2003JD003887.

Lohmann, U. and J. Feichter (2005), Global indirect aerosol effects: a review, *Atmos. Chem. Phys., 5*, 715–737, SRef-ID: 1680-7324/acp/2005-5-715.

Lugauer, M., U. Baltensperger, M. Furger, H. W. Gäggeler, D. T. Jost, M. Schwikowski, and H. Wanner (1998), Aerosol transport to the high Alpine sites Jungfraujoch (3454 m a.s.l.) and Colle Gnifetti (4452 m a.s.l.), *Tellus, 50B,* 76–92.

Marshall, J. S. and Palmer, W. M. (1948), The distribution of raindrop with size, *J. Meteor., 5,* 165–166, 1948.

Mäkelä J. M., P. Aalto, V. Jokinen, T. Pohja, A. Nissinen, S. Palmroth, T. Markkanen, K. Seitsonen, H. Lihavainen, and M. Kulmala (1997), Observations of ultrafine aerosol particle formation and growth in boreal forest, *Geophys. Res. Lett., 24*, 1219–1222

McNaughton, C. S., A. D. Clarke, S. G. Howell, K. G. Moore II, V. Brekhovskikh, R. J. Weber, D. A. Orsini, D. S. Covert, G. Buzorius, F. J. Brechtel, G. R. Camichael, Y. Tang, F. L. Eisele, R. L. Mauldin, A. R. Brandy, D. C. Thornton, and B. Blomquist (2004), Spatial distribution and size evolution of particles in Asian outflow: Significance of primary and secondary aerosols during ACE-Asia and TRACE-P, *J. Geophys. Res., 109,* D19S06, doi: 10.1029/2003JD003528.

Mendonca, B. G. (1969), Local wind circulation on the slopes of Mauna Loa, *J. Appl. Meteorol., 8,* 533–541.

Mircea, M., and S. Stefan (1998), A theoretical study of the microphysical parameterization of the scavengning coefficient as a function of precipitation type and rate, *Atmos. Environ., 32,* 2931–2938.

Mönkkönen, P, I. K. Koponen, K. E. J. Lehtinen, K. Hämeri, R. Uma, and M. Kulmala (2005), Measurements in a highly polluted Asian mega city: observations of aerosol number size distribution, modal parameters and nucleation events, *Atmos. Chem. Phys., 5,* 57–66, 2005, SRef-ID: 1680-7324/acp/2005-5-57.

Mukai, H., Y. Ambe, and K. Shibata (1990), Long-term variation of chemical composition of atmospheric aerosol on the Oki Islands in the Sea of Japan, *Atmos. Environ.*, *24A*, 1379–1390.

Napari, I, M. Noppel, H. Vehkamäki, and M. Kulmala (2002), An improved model for ternary nucleation of sulfuric acid-ammonia-water, *J. Chem. Phys.*, *116*, 4221–4227.

Nilsson, E. D., Ü. Rannik, M. Kulmala, G. Buzorious, and C. D. O'Dowd (2001a), Effects of continental boundary layer evolution, convection, turbulence and entrainment, on aerosol formation, *Tellus*, *53B*, 441–461.

Nilsson, E. D., J. Paatero, and M. Boy (2001b), Effects of air masses and synoptic weather on aerosol formation in the continental boundary layer, *Tellus*, *53B*, 462–478.

Nilsson, E. D., and M. Kulmala (2006), Aerosol formation over the Boreal forest in Hyytiälä, Finland: monthly frequency and annual cycles – the roles of air mass characteristics and synoptic scale meteorology, *Atmos. Chem. Phys. Discuss.*, *6*, 10425–10462.

Noppel, M. H., Vehkamaki, M. Kulmala (2002), An improved model for hydrate formation in sulfuric acid–water nucleation, *J. Chem. Phys. 116,* 218–228.

Nyeki, S., F. Li, E. Weingartner, N. Streit, I. Colbeck, H. W. Gäggeler, and U. Baltensperger (1998), The background aerosol size distribution in the free troposphere: An analysis of the annual cycle at a high-alpine site, *J. Geophys. Res., 103,* 31747–31761.

O'Dowd, C. D., M. Greever, M. K. Hill, M. H. Smith, and S. G. Jennings (1998), New particle formation: Nucleation rates & spatial scales in the clean marine coastal environment, *Geophys. Res. Lett., 24,* 1661–1664

O'Dowd, C. D., J. L. Jimenez, R. Bahreini, R. C. Flagan, J. H. Seinfeld, K. Hämeri, L. Pirjola, M. Kulmala, S. G. Jennings, and T. Hoffmann (2002a), Marine aerosol formation from biogenic iodine emissions, *Nature, 417,* 632–636.

O'Dowd, C. D., P. Aalto, K. Hämeri, M. Kulmala, and T. Hoffmann (2002b), Atmospheric particles from organic vapours, *Nature*, *416*, 497–498.

Okita, T., H. Hara, N. Fukuzaki (1996), Measurements of atmospheric SO_2 and SO_4^{2-}, and determination of the wet scavenging coefficient of sulfate aerosols for the winter monsoon season over the Sea of Japan, *Atmos. Environ., 30,* 3733–3739.

Osada, K., M. Kido, C. Nishita, K. Matsunaga, Y. Iwasaka, M. Nagatani, and H. Nakada

(2002), Changes in ionic constituents of free tropospheric aerosol particles obtained at Mt. Norikura, *Atmos. Environ., 36,* 5469–5477.

Osada, K., M. Kido, H. Iida, K. Matsunaga, Y. Iwasaka, M. Nagatani, and H. Nakada (2003), Seasonal variation of free tropospheric aerosol particles at Mt. Tateyama, central Japan, *J. Geophys. Res., 108,* 8667, doi:10.1029/2003JD003544.

Osada, K., M. Kido, C. Nishita, K. Matsunaga, Y. Iwasaka, M. Nagatani, and H. Nakada (2007), Temporal variation of water-soluble ions of free tropospheric aerosol particles over central Japan, *Tellus, 59B,* 742-754.

Pruppacher, H. R. and J. D. Klett (1997), *Microphysics of clouds and precipitation,* Kluwer Academic Publishers, Boston.

Raes, F. (1995), Entrainment of free tropospheric aerosols as a regulating mechanism for cloud condensation nuclei in the remote marine boundary layer, *J. Geophys. Res., 100,* 2893–2903.

Raes, F., R. Van Dingenen, E. Cuevas, P. F. J. Van Velthoven, and J. M. Prospero (1997), Observations of aerosols in the free troposphere and marine boundary layer of the subtropical Northeast Atlantic: Discussion of processes determining their size distribution, *J. Geophys. Res.*, *102*, 21315–21328.

Raes, F., R. Van Dingenen, E. Vignati, J. Wilson, J.-P. Putaud, J. H. Seinfeld, and P. Adams (2000), formation and cycling of aerosols in the global troposphere, *Atmos. Environ., 34,* 4215–4240.

Rolph, G. D. (2003), Real-time Environmental Applications and Display system (READY) Website (http://www.arl.noaa.gov/ready/hysplit4.html). NOAA Air Resources Laboratory, Silver Spring, MD.

Sakai, T., T. Shibata, S. A. Kwon, Y. S. Kim., K. Tamura, and Y. Iwasaka (2000), Free tropospheric aerosol backscatter, depolarization ratio, and relative humidity measured with the Raman lidar at Nagoya in 1994–1997: contributions of aerosols from the Asian Continent and the Pacific Ocean, *Atmos. Environ., 34,* 431–442.

Scott, B. C. (1982), Theoretical estimates of the scavenging coefficient for soluble aerosol particles as a function of precipitation type, rate and altitude, *Atmos. Environ.*, *16*, 1753–1762.

Seinfeld, J. H. and S. N. Pandis (2006), *Atmospheric Chemistry and Physics: From Air*

Pollution to Climate Change, –2nd ed., John Wiley&Sons, Inc., Hoboken, New Jersey.

Shaw, G. E. (2007), Aerosols at a mountaintop observatory in Arizona, *J. Geophys. Res.*, *112*, D07206, doi:10.1029/2005JD006893.

Sirois, A., and L. A. Barrie (1999), Arctic lower tropospheric aerosol trends and composition at Alert, Canada: 1980–1995, *J. Geophys. Res.*, *104*, 11599–11618.

Siebert, H., F. Stratmann, and B. Wehner (2004), First observation of increased ultrafine particle number concentrations near the inversion of a continental planetary boundary layer and its relation to ground-based measurements, *Geophys. Res. Lett.*, *31*, L09102, doi:10.1029/2003GL019086.

Slinn, W. G. N. (1983) Precipitation scavenging, in *Atmospheric Sciences and Power Production–1979*, Chap. 11, Division of Biomedical Environmental Research, U.S. Department of Energy, Washington, DC.

Sogacheva, L., A. Hamed, M. C. Facchini, M. Kulmala, and A. Laaksonen (2007), Relation of air mass history to nucleation events in Po Valley, Italy, using back trajectories analysis, *Atmos. Chem. Phys.*, *7*, 839–853.

Sparmacher, H., K. Fülber, and H. Bonka (1993), Blow-cloud scavenging of aerosol particles: Particle-bound radio nuclides – Experimental, *Atmos. Environ., 27A*, 605–618.

Stanier, C. O., A. Y. Khlystov, and S. N. Pandis (2004), Nucleation events during the Pittsburg Air Quality Study: Description and relation to key meteorological, gas phase, and aerosol parameters, *Aerosol Sci. Technol., 38S,* 253–264.

Streets, D. G., T. C. Bond, G. R. Carmichael, S. D. Fernandes, Q. Fu, D. He, Z. Klimont, S. M. Nelson, N. Y. Tsai, M. Q. Wang, J. –H. Woo, and K. F. Yarber (2003), An inventory of gaseous and primary aerosol emissions in Asia in the year 2000, *J. Geophys. Res., 108*(D21), 8809, doi:10.1029/2002JD003093.

Stratmann, F., H. Siebert, G. Spindler, B. Wehner, D. Althausen, J. Heintzenberg, O. Hellmuth, R. Rinke, U. Schmieder, C. Seidel, T. Tuch, U. Uhrner, A. Wiedensohler, U. Wandinger, M. Wendisch, D. Schell, and A. Stohl (2003), New-particle formation events in a continental boundary layer: first results from the SATURN experiment, *Atmos. Chem. Phys.*, *3*, 1445–1459.

Tunved, P., H.-C. Hansson, V.-M. Kerminen, J. Ström, M. Dal Maso, H. Lihavainen, Y. Viisanen, P. P. Aalto, M. Komppula, and M. Kulmala (2006), High natural aerosol

loading over boreal forests, *Science*, *312*, doi:10.1126/science.1123052.

Twomey, S. (1977), *Atmospheric Aerosols,* Elsevier Scientific Publishing Company, New York.

Tang, T. N. and H. R. Munkelwitz (1994), Water activities, densities, and refractive indices of aqueous sulfates and sodium nitrate droplets of atmospheric importance, *J. Geophys. Res. 99*, 18801–18808.

Tsutsumi, Y., Y. Makino, and J. Jensen (1996), Aircraft measurements of tropospheric ozone over the Western Pacific Ocean, *Atmos. Environ., 30,* 1763–1772.

Tsutsumi, Y., Y. Igarashi, Y. Zaizen, and Y. Makino (1998), Case studies of tropospheric ozone events observed at the summit of Mount Fuji, *J. Geophys. Res.*, *103*, 16935–16951.

Tunved, P., J. Ström, and H. -C. Hanson (2004), An investigation of processes controlling the evolution of the boundary layer aerosol size distribution properties at the Swedish background station Aspvreten, *Atmos. Chem. Phys., 4,* 2581–2592, SRef-ID: 1680-7324/acp/2004-4-2581.

Tunved, P., E. D. Nilsson, H.-C. Hansson, and J. Ström (2005), Aerosol characteristics of air masses in northern Europe: Influence of location, transport, sinks, and sources, *J. Geophys. Res., 110,* D07201, doi:10.1029/2004JD005085.

Twomey, S. (1977), *Atmospheric Aerosols*, Elsevier Scientific Publishing Company, New York.

Vana, M., M. Kulmala, M. Dal Maso, U. Hõrrak, and E. Tamm (2004), Comparative study of nucleation mode aerosol particles and intermediate air ions formation events at three sites, *J. Geophys. Res.*, *109*, D17201, doi:10.1029/2003JD004413.

Wang, P. K., S. N. Grover, and H. R. Pruppacher (1978), On the effect of electric charges on the scavengning of aerosol particles by clouds and small raindrops, *J. Atmos. Sci., 35,* 1735–1743.

Wang, P. K., amd H. R. Pruppacher (1977), An experimental determination of the efficiency with which aerosol particles are collected by water drops in subsaturated air, *J. Atmos. Sci., 34,* 1664–1669.

Warneck, P. (1999), *Chemistry of the natural atmosphere, Second Edition,* p 630, Academic Press Inc., San Diego.

Weber, R. J., P. H. McMurry, F. J. Eisele, and D. J. Tanner (1995), Measurement of expected nucleation precursor species and 3–500-nm diameter particles at Mauna Loa Observatory, Hawaii, *J. Atmos. Sci.*, *52*, 2242–2257.

Weber, R. J., J. J. Marti, P. H. McMurry, F. L. Eisele, D. J. Tanner, and A. Jefferson (1997), Measurements of new particle formation and ultrafinr particle growth rates at a clean continental site, *J. Geophys. Res., 102,* 4375–4385.

Wehner, B., H. Siebert, F. Stratmann, T. Tuch, A. Wiedensohler, T. Petäjä, M. Dal Maso, and M. Kulmala (2007), Horizontal homogeneity and vertical extent of new particle formation events, *Tellus*, *59B*, 362–371.

Weingartner, E., S. Nyeki, and S. Baltensperger (1999), Seasonal and diurnal variation of aerosol size distributions ($10 < D < 750$ nm) at a high-alpine site (Jungfraujoch 3580 m asl), *J. Geophys. Res.*, *104*, 26809–26820.

Whitby, K.T. (1978), The physical characteristics of sulfur aerosols, *Atmos. Environ., 12*, 135–159.

Wu, Z., M. Hu, S. Liu, B. Wehner, S. Bauer, A. Ma ßling, A. Wiedensohler, T. Petäjä, M. Dal Maso, and M. Kulmala (2007), New particle formation in Beijing, China: Statistical analysis of a 1-year data set, *J. Geophys. Res.*, *112*, D09209, doi:10.1029/2006JD007406.

Yu, F., and R. P. Turco (2000), Ultrafine aerosol formation via ion-mediated nucleation, *Geophys. Res. Lett.*, *27*, 883–886.

Yu, F. (2006a), Binary H_2SO_4-H_2O homogenous nucleation based on kinetic quasi-unary nucleation model: Look-up tables, *J. Geophys. Res., 111,* D04201, doi:10.1029/2005JD006358.

Yu, F. (2006b), From molecular clusters to nanoparticles: second-generation ion-mediated nucleation model, *Atmos. Chem. Phys., 6,* 5193–5211.

Yu, F. (2006c), Effect of ammonia on new particle formation: A kinetic H_2SO_4-H_2O-NH_3 nucleation model constrained by laboratory measurements, *J. Geophys. Res., 111,* D01204, doi:10.1029/2005JD005968.

Yu, H., Y. J. Kaufman, M. Chin, G. Feingold, L. A. Remer, T. L. Anderson, Y. Balkanski, N. Bellouin, O. Boucher, C. Christopher, P. DeCola, R. Kahm, N. Loeb, M. S. Reddy, M. Schulz, T. Takemura, and M. Zhou (2006), A review of measurement-based assessments

of the aerosol direct radiative effect and forcing, *Atmos. Chem. Phys.*, *6*, 613–666.

Zaizen, Y., K. Okada, M. Ikegami, Y. Sawa, and Y. Makino (2004), Number-size distributions of Aerosol particles in the free troposphere over the northwestern Pacific Ocean – Influence of Asian Outflow and tropical air transport, *J. Meteor. Soc. Japan, 82,* 1147–1160.

Zhang, R. et al. (2004), Atmospheric new particle formation enhanced by organic acids, *Science, 304,* 1487–1490.

Table 3-1. Backward Trajectory, Median Cumulative Precipitation Amount, and Local Precipitation Rate for Different Air Mass Types[a]

Type	Five-Day Trajectory	Cumulative Precipitation Rate, mm	Local Precipitation Rate, $mm \cdot h^{-1}$	Number of Hourly Data
A-1	Pacific Ocean	0.9 [0.2–1.4]	0 [0–0]	26
A-2	Pacific Ocean	10 [8.0–17]	0 [0–0]	48
B-1	Other	0.2 [0.1–0.7]	0 [0–0]	125
B-2	Other	0.7 [0–2.6]	2.3 [0.5–4.0]	29

[a]Cumulative precipitation amounts are defined as cumulative precipitation amount for the preceding 24 h before arrival estimated from precipitation rate (objective analysis data) along backward trajectories. Values in square brackets indicate 25–75% ranges.

Table 3-2. Median Values of Log-normal Parameters Obtained by Log-normal Fitting on Hourly Size Distributions[a]

Mode	Type	$D_{p,g}$, nm	N, cm^{-3}	$_g$	FO, %
Accumulation mode	A-1	140 [120–170]	350 [140–580]	1.43 [1.34–1.57]	100
	B-1	120 [100–140]	400 [200–590]	1.71 [1.58–1.81]	86
	A-2	140 [110–160]	97 [53–130]	1.41 [1.33–1.59]	54
	B-2	110 [100–120]	94 [35–420]	1.45 [1.35–1.62]	38
Aitken mode	A-1	53 [51–64]	890 [610–1100]	1.47 [1.40–1.52]	100
	B-1	54 [44–71]	230 [130–310]	1.55 [1.37–1.80]	59
	A-2	52 [40–61]	160 [100–610]	1.50 [1.44–1.76]	98
	B-2	56 [47–61]	336 [200–600]	1.44 [1.38–1.57]	97
Nucleation mode	All	25 [22–28]	53 [33–87]	1.34 [1.23–1.44]	14

[a]Values in square brackets indicate 25–75% ranges. FO denotes frequency of occurrence of the mode.

Table 4–1. Average *CS*, SO_2, and NH_3 Concentrations on the NPF Event Day and Non-Event Sunny Day[a]

	CS, $10^{-3}s^{-1}$		SO_2, ppbv	NH_3, ppbv	
	4–8 h	12–16 h	Afternoon hours [b]	4–11 h	10–17 h
NPF event day	0.6 [0.6–0.6]	2.0 [1.5–2.2]	0.16 [0.10–0.23]	0.16 [0.14–0.17]	0.33 [0.29–0.37]
Non-event sunny day	1.2 [0.6–1.6]	3.8 [3.1–4.2]	0.25 [0.07–0.34]	0.33 [0.16–0.43]	0.40 [0.23–0.43]

a: Values in square brackets are 25–75% ranges.

b: Impregnated filter samples obtained within 10–17 h LT during September 2001, and average concentrations in 12–16 h during August–September 2002.

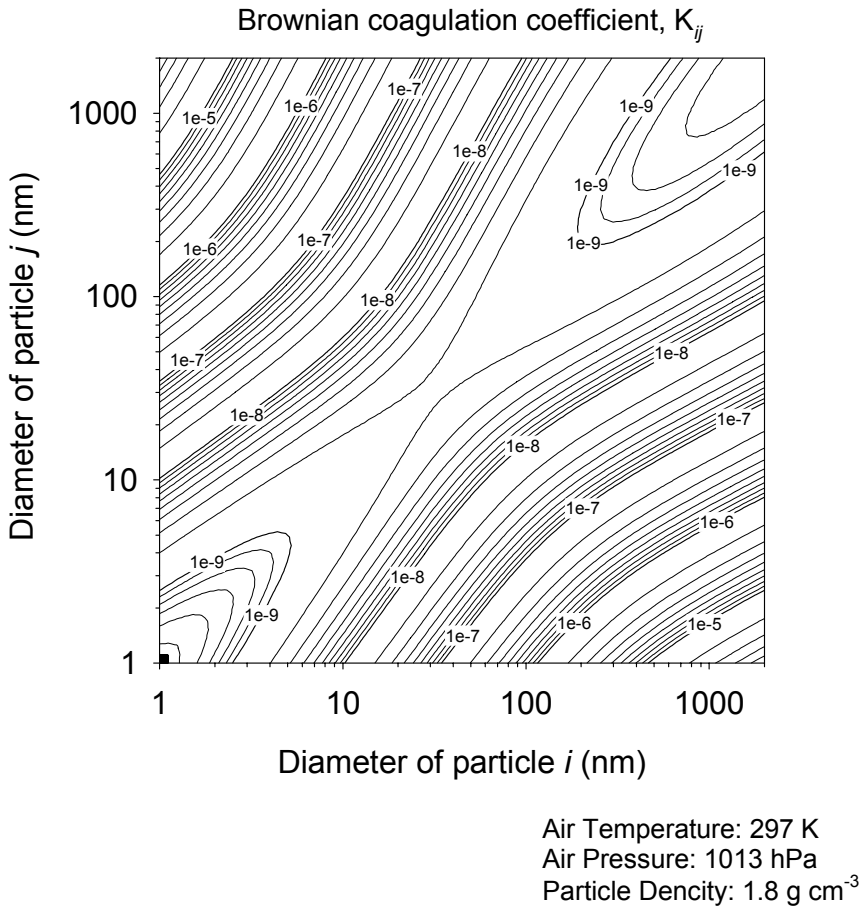

Figure 1-1. Brownian coagulation coefficient K_{ij} (cm^3 s^{-1}) for coagulation of particles of diameters D_i and D_j in air at 297 K and 1013 hPa based on Fuchs [1964].

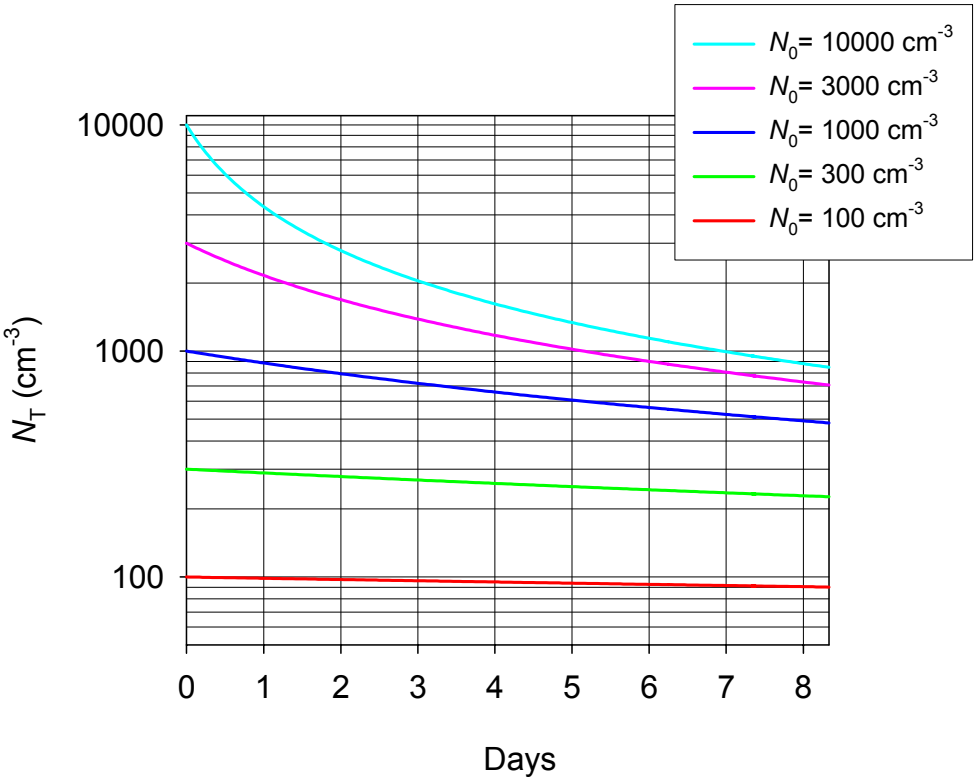

Figure 1-2. Time evolution of particle number concentration by the coagulation predicted by the equation (1-4) for the coagulational coefficient, K=3*10^{-9} cm^3 s^{-1}.

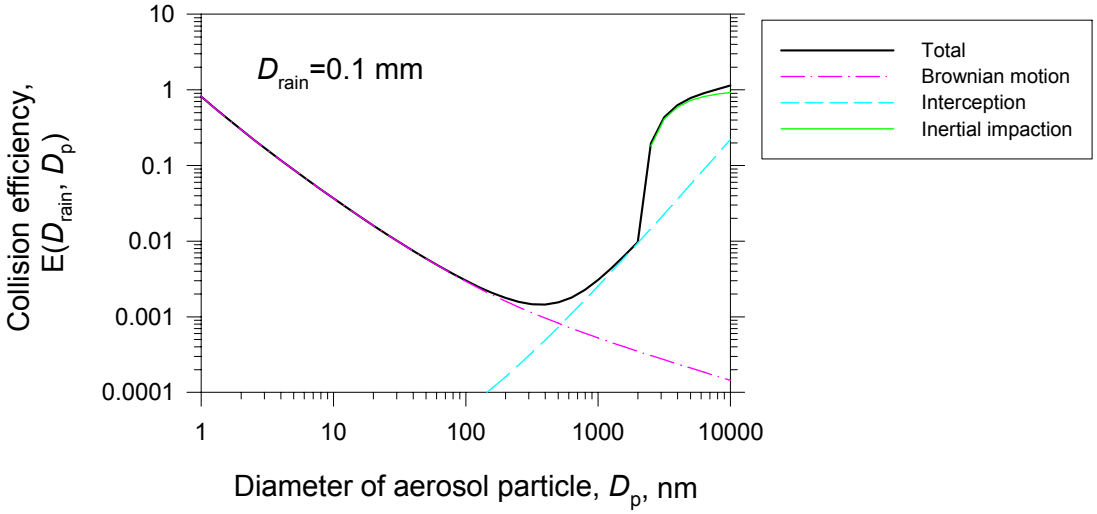

Figure 1-3. Collision efficiency, E, of a raindrop of diameter 0.1 mm as a function of the collected aerosol particle diameter, D_p, based on Slinn (1983): Total (black solid line), Brownian motion (pink solid line with dots), Interception (blue dashed line), and Impaction (green solid line).

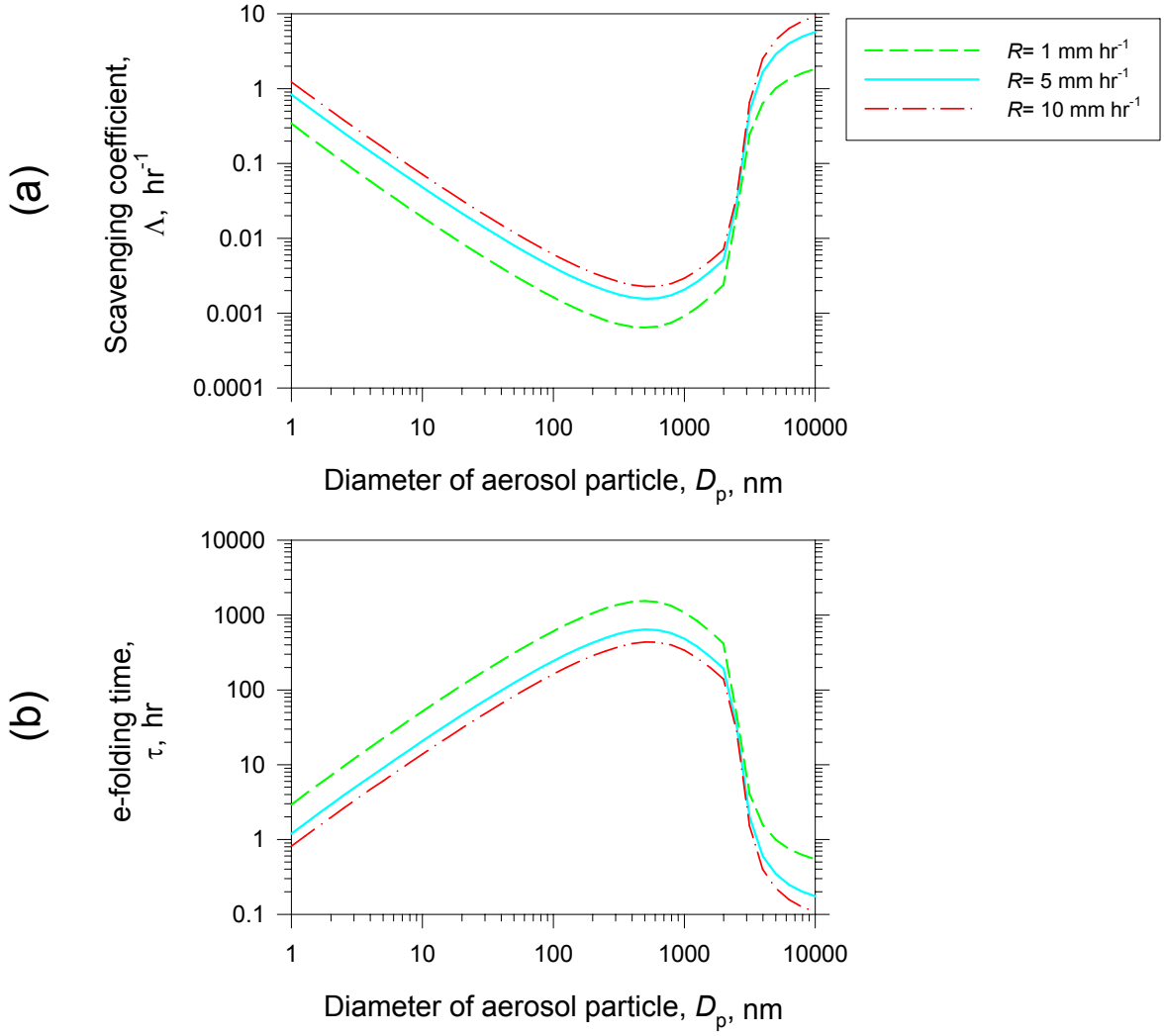

Figure 1-4. (a) Scavenging coefficient, Λ, and (b) e-folding time, τ, for the raindrop size distribution of Marshall and Palmer (1948): precipitation rate, R=1 mm hr^{-1} (green broken line), R=5 mm hr^{-1} (blue solid line), and R=10 mm hr^{-1} (red solid line with dots).

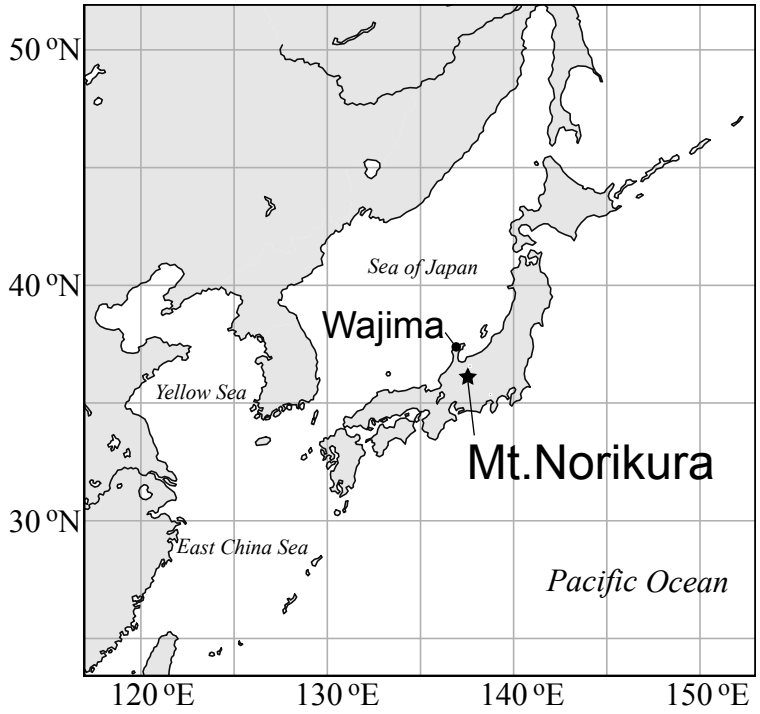

Figure 2-1. Location of the Norikura Observatory (2770 m a.s.l.) of ICRR, University of Tokyo at Mt. Norikura and aerological observatory, Wajima.

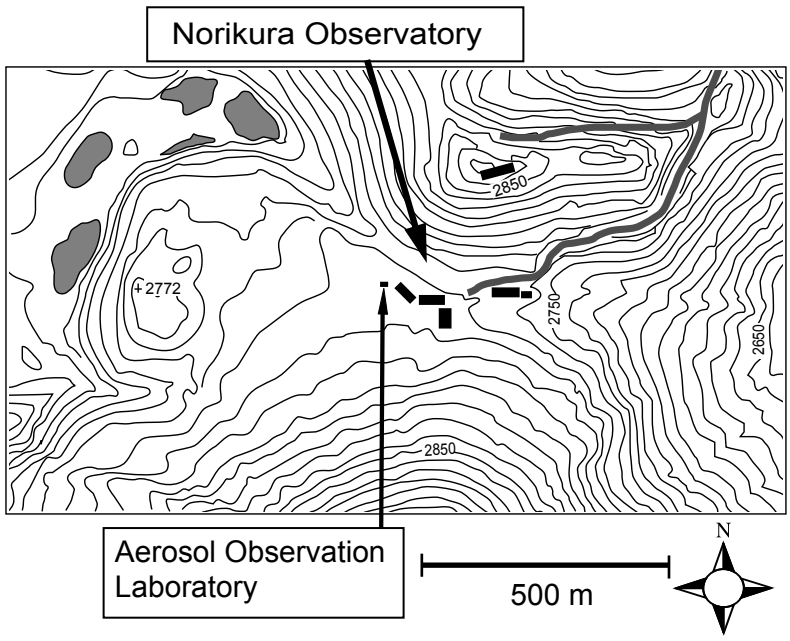

Figure 2-2. The location of the aerosol observation laboratory and local topography.

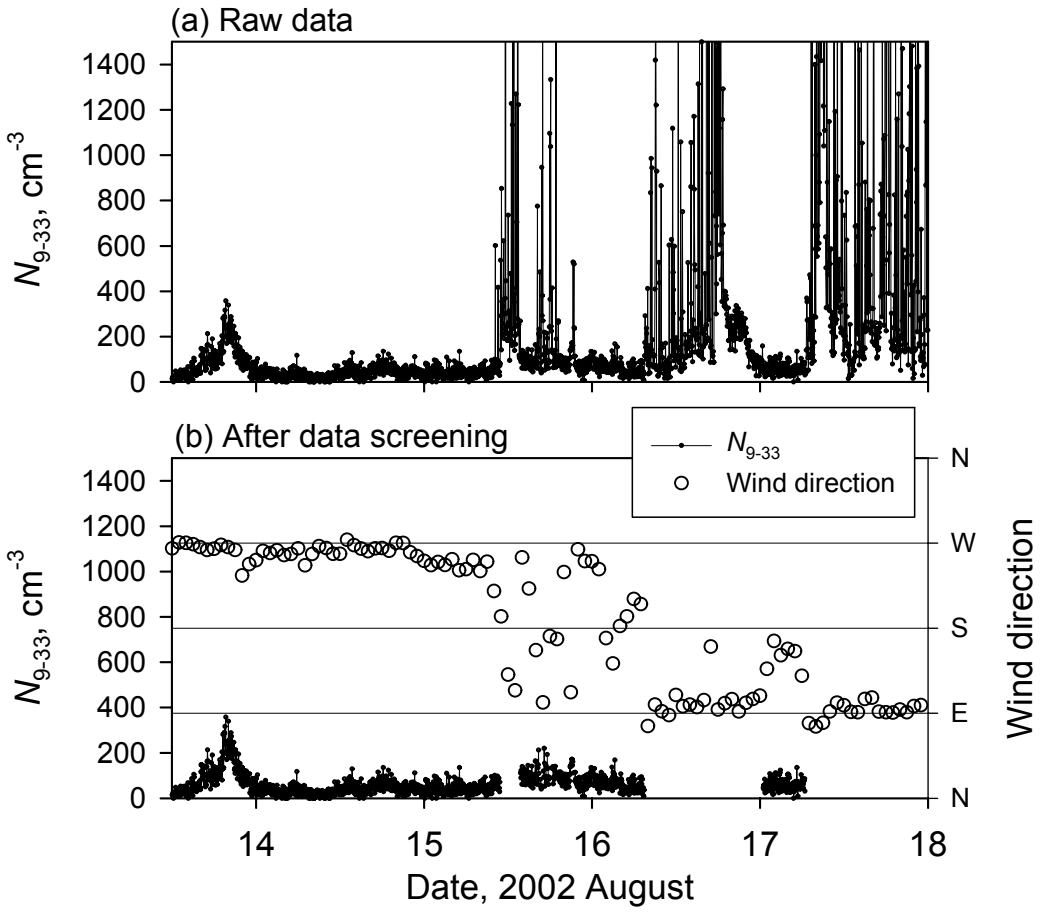

Figure 2-3. Temporal variations of particle concentration in sizes of $9 < D_p < 33$ nm ($N_{9\text{-}33}$): (a) raw data, and (b) the data after emilimination of the infuluence of local air contaminations accoring to local wind direction.

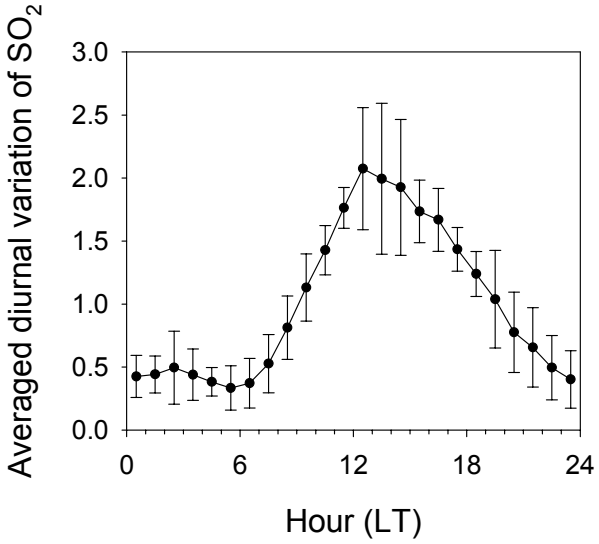

Figure 3-1. Average diurnal variation of SO_2 concentration during eight clear summer days. The SO_2 data were normalized; daily average values were set to unity. Bars indicate the standars deviation.

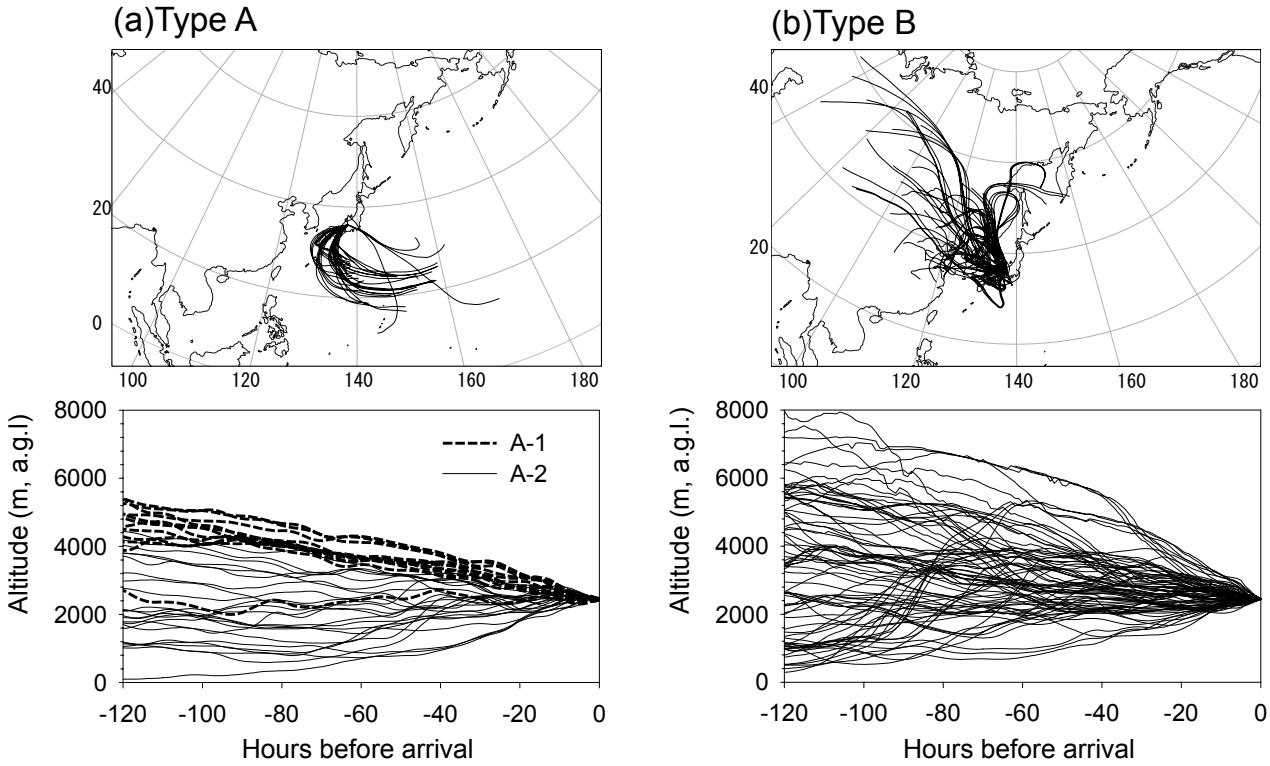

Figure 3-2. (a) Horizontal (top) amd vertical (bottom) backward trajectories for five days of type A(type A-1, thick broken lines: type A-2, thin lines) and (b) type B.

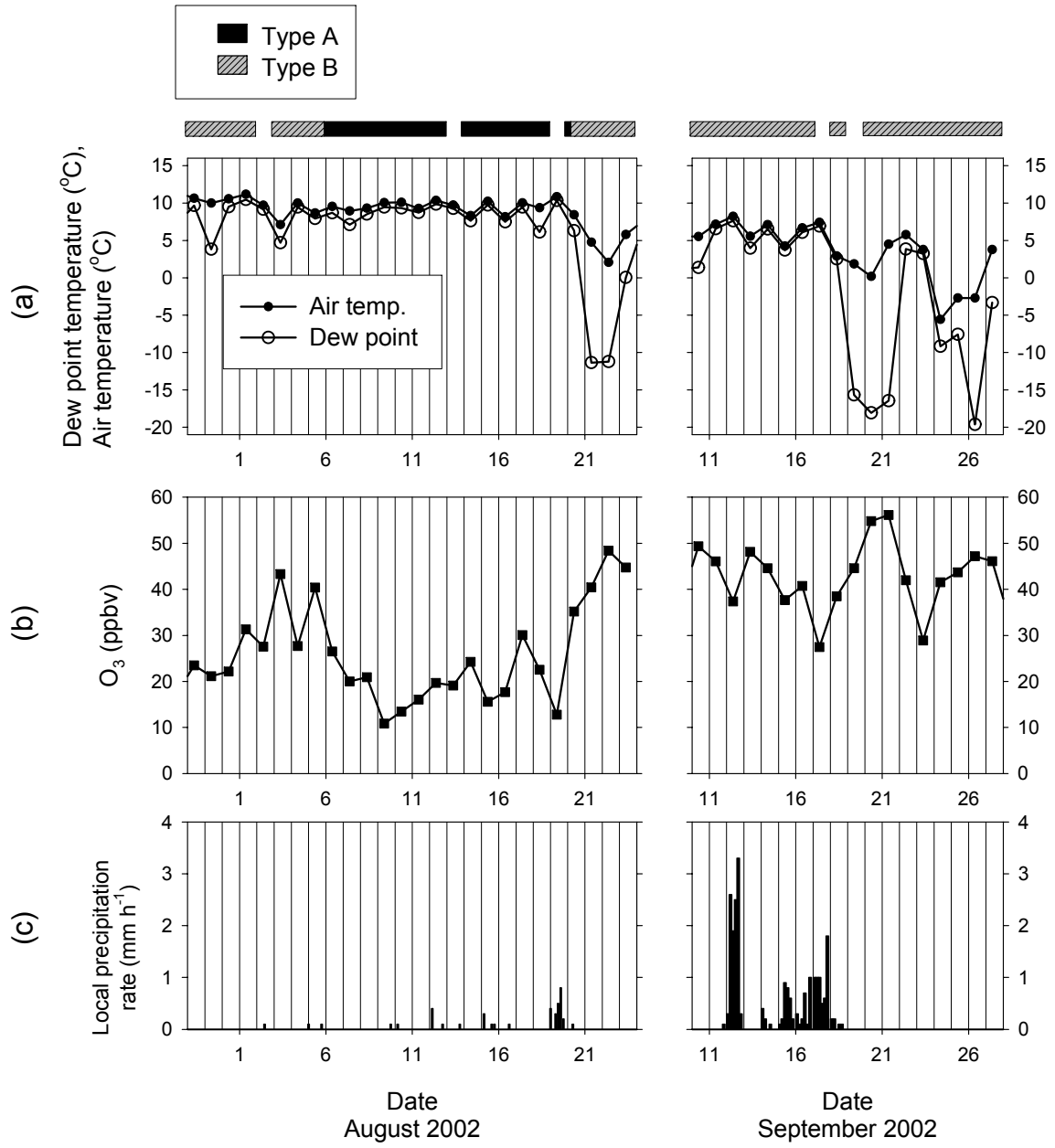

Figure 3-3. (a) Temporal variations of ambient air and dew point temperatures, (b) O_3 concentration, and (c) precipitation rate in free tropospheric condition (0:00-6:00 LT). Periods of types A and B are depicted as black and shaded gray bars, respectively, at the top of Figure 3-3a.

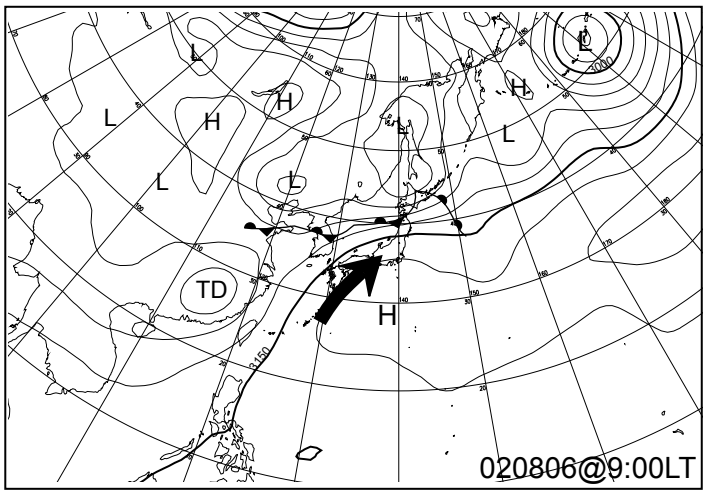

Figure 3-4. Seven hundred hectopascals geopotential height (m) fields on 6 August 2002 showing an examples of synoptic-scale meteorological condition of type A. Location of fronts on surface are superimposed on the map.

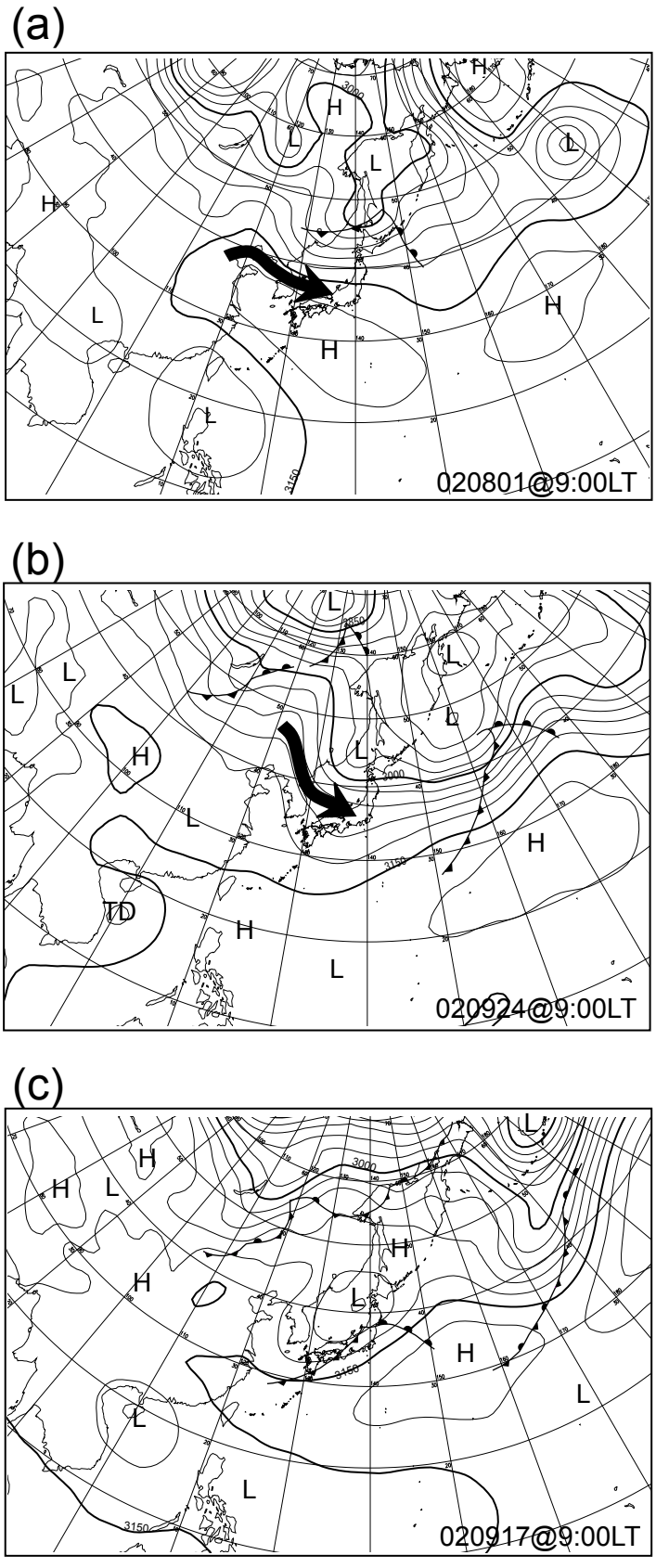

Figure 3-5. (a) Seven hundred hectopascals geopotential height (m) field on 1 August, (b) 24 September, and (c) 17 September 2002 showing examples of synoptic-scale meteorological conditions of type B. Location of fronts on surface are superinposed on the maps.

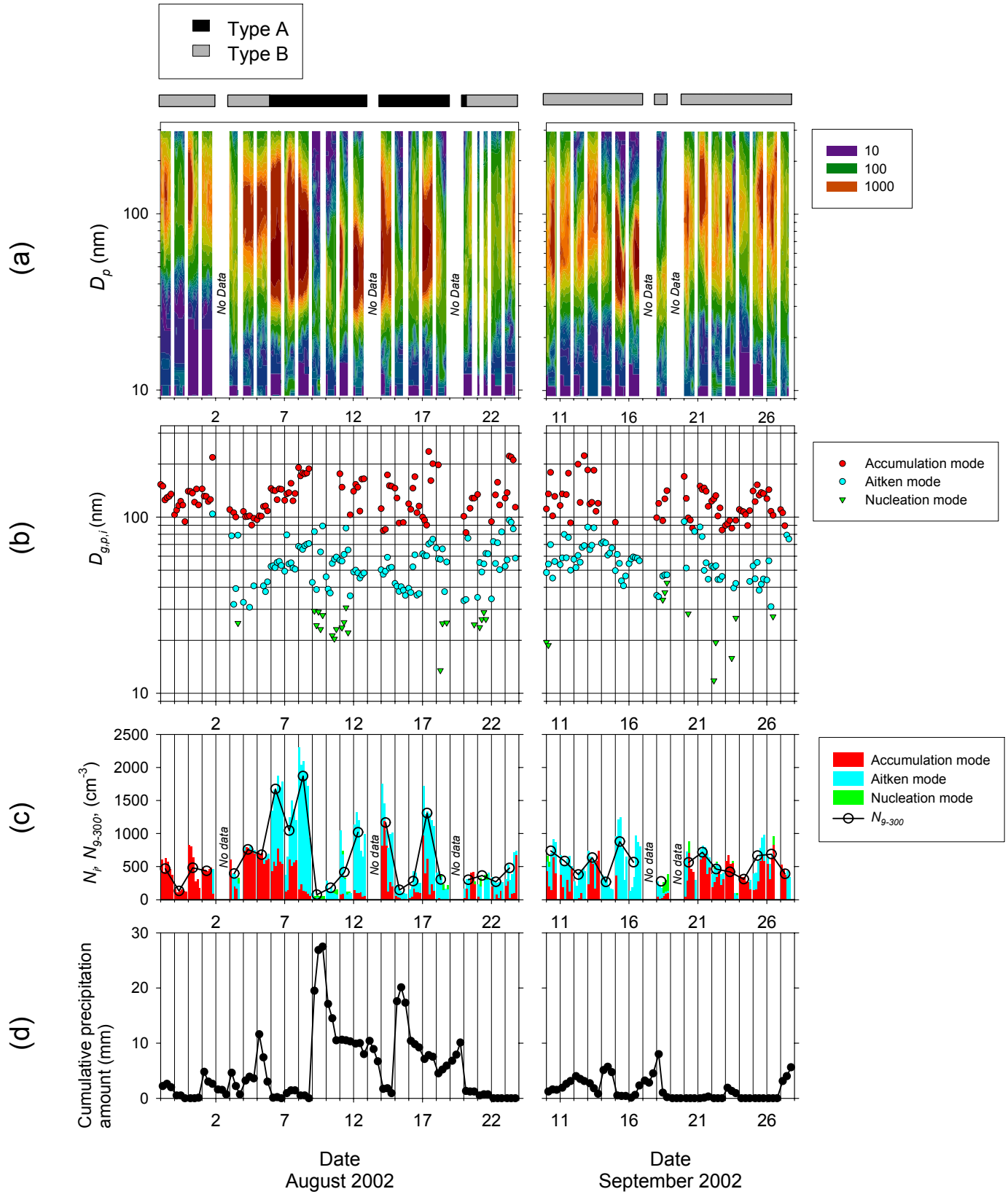

Figure 3-6. (a) Temporal variations of number-size distribution of free tropospheric particles in dN/dlogD_p (cm^{-3}), (b) geometric mean diameter of mode, (c) modal particle concentrations (bars) and total particle concentration for 9-300 nm diameter, $N_{9\text{-}300}$ (cirlcles), (d) cumulative precipitation amount in air mass for the last 24 h before arrival. The periods of types A and B are designated by black and gray bars, respectively, at top of the contour maps.

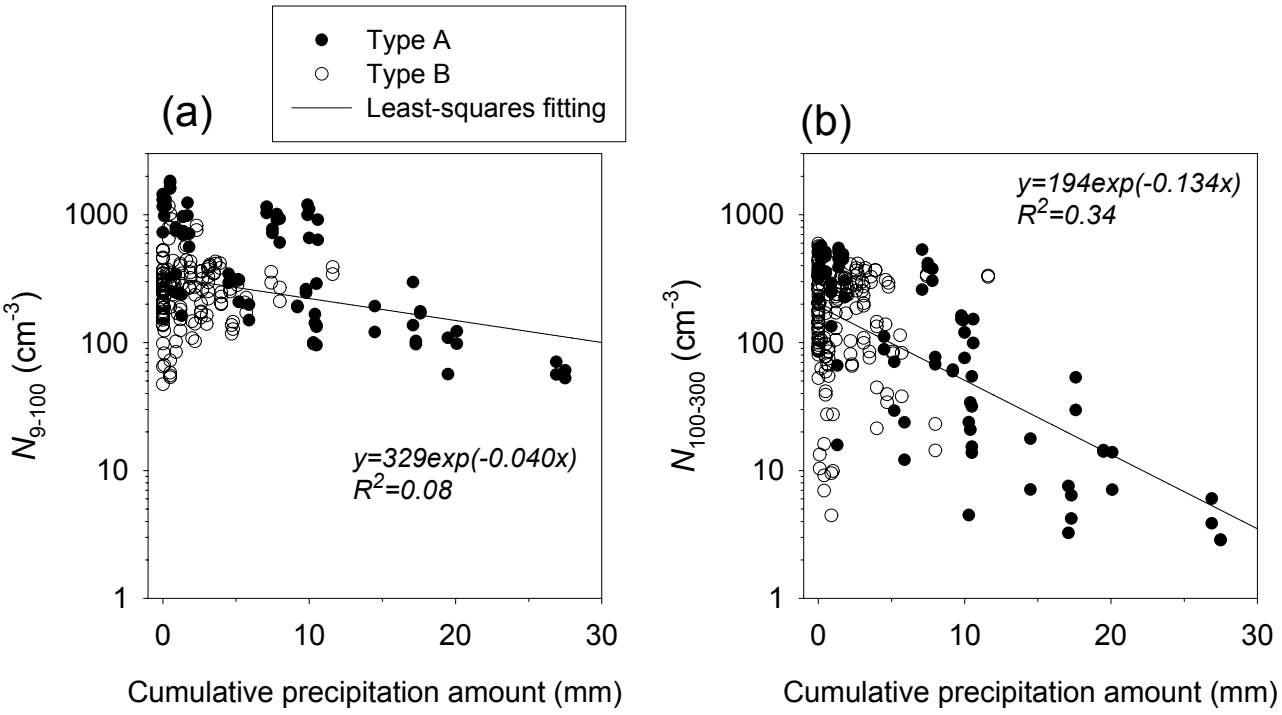

Figure 3-7. (a) Relationship of $N_{9\text{-}100}$ and (b) $N_{100\text{-}300}$ with cumulative precipitation amount in air mass. Black and white circles denote the types A and B air masses, respectively. Lines are least squares fitting line by exponential function.

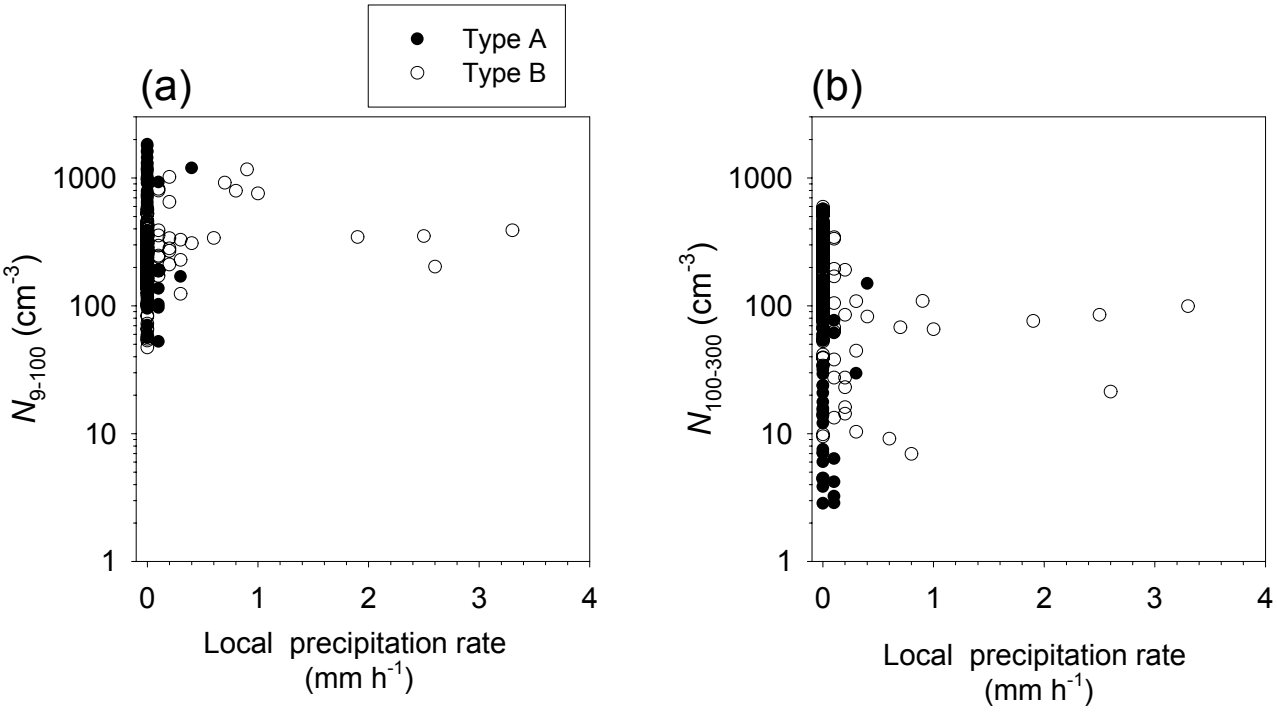

Figure 3-8. (a) Scatterplots of $N_{9\text{-}100}$ and (b) $N_{100\text{-}300}$ versus local precipitation rate. Black and white circles denote data of the types A adn B air masses, respectively.

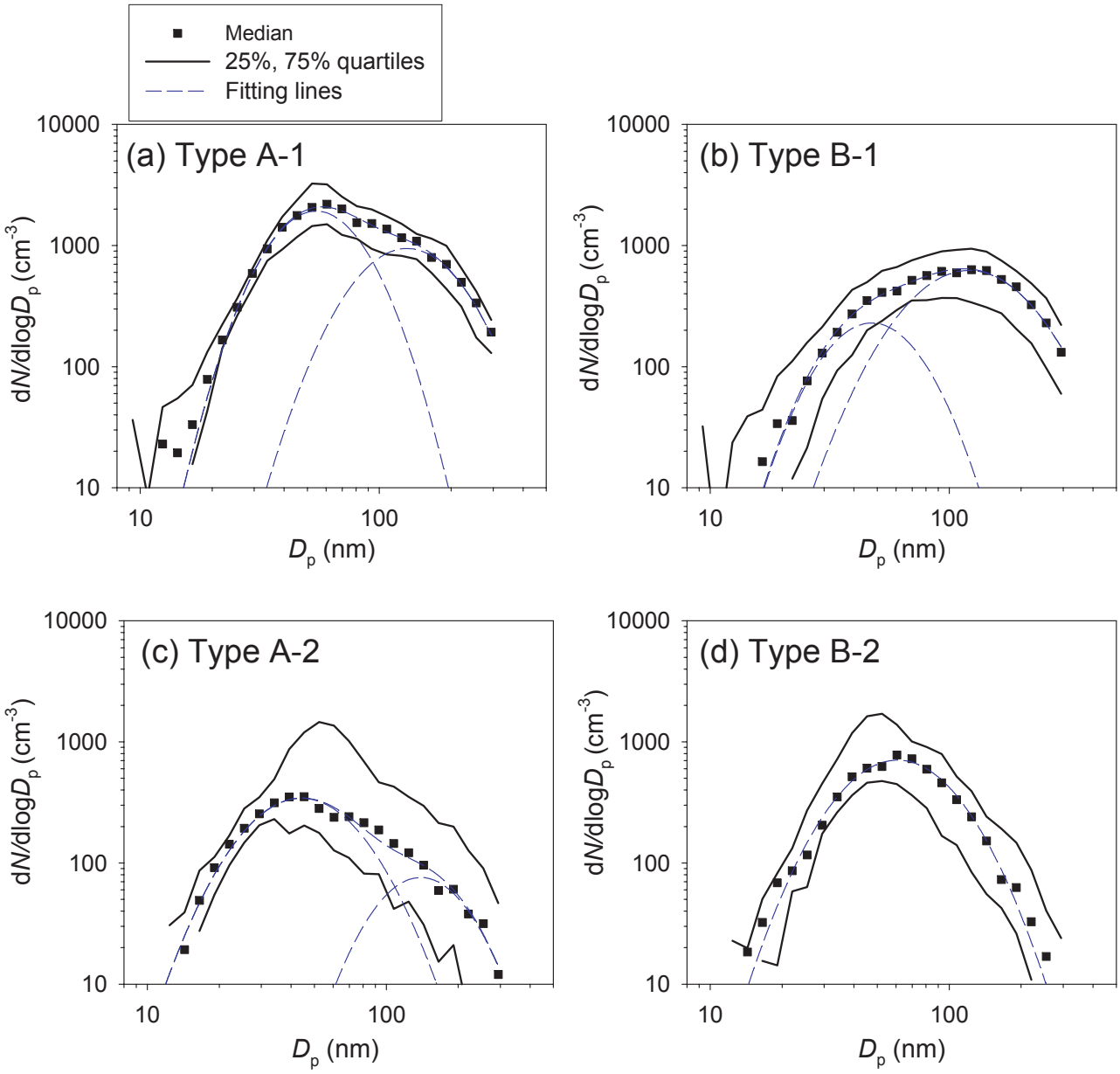

Figure 3-9. (a) Median number-size distributions of type A-1, (b) type B-1, (c) type A-2, and (d) type B-2. Thick lines indicate 25-75% quatile ranges. Broken blue lines are fitting lines for the median number-size distributions by lognormal distributions.

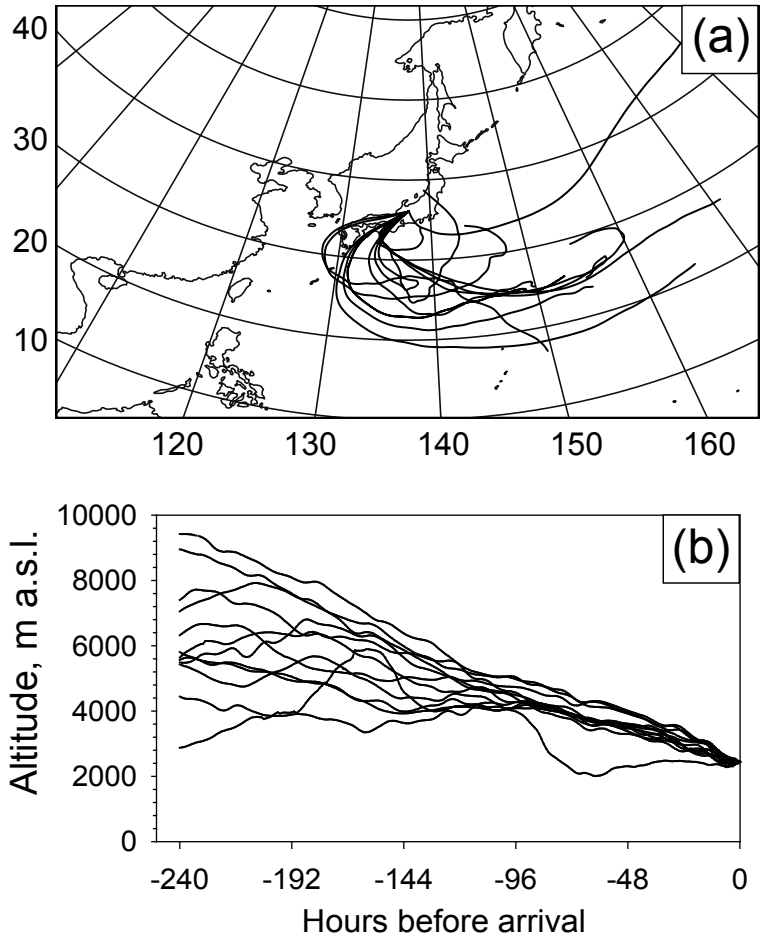

Figure 3-10. (a) Horizontal and (b) vertical backward trajectories for 10 days of air mass type A-1.

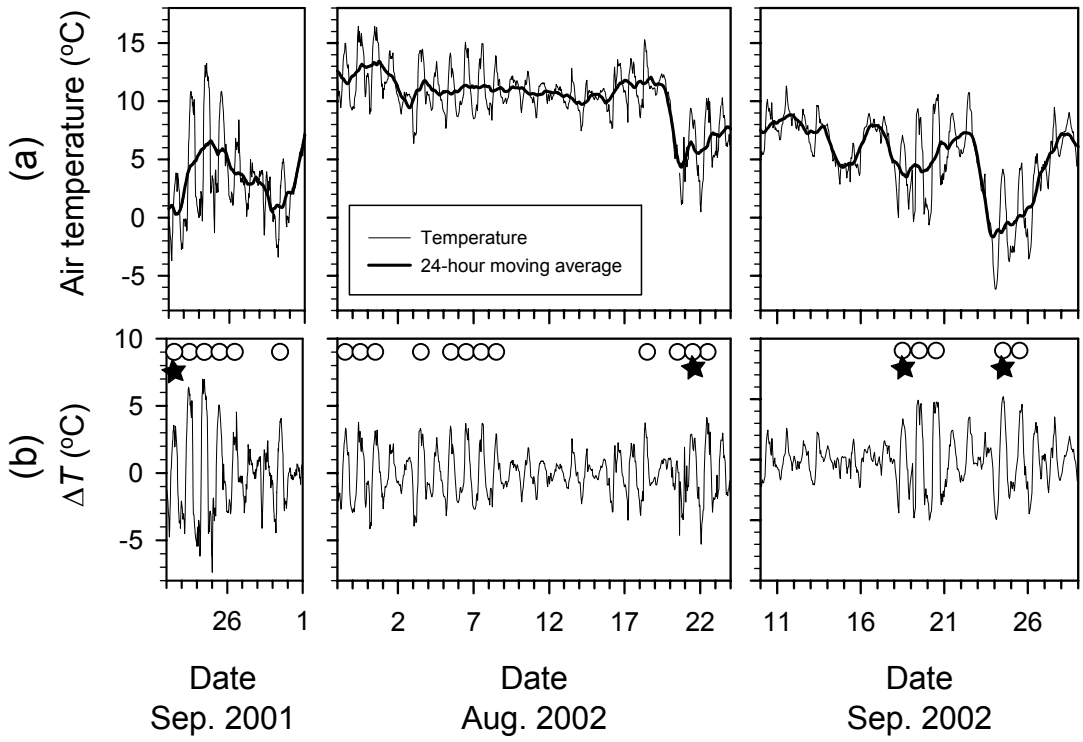

Figure 4-1. Temporal variation of (a) hourly air temperature (thin line) and its 24-h moving average (thick line) at Mt. Norikura; (b) the deviation of hourly air temperature from the 24-h moving average (ΔT). Circles and star symbols in Fig. 4-1b respectively signify the sunny days and NPF event days

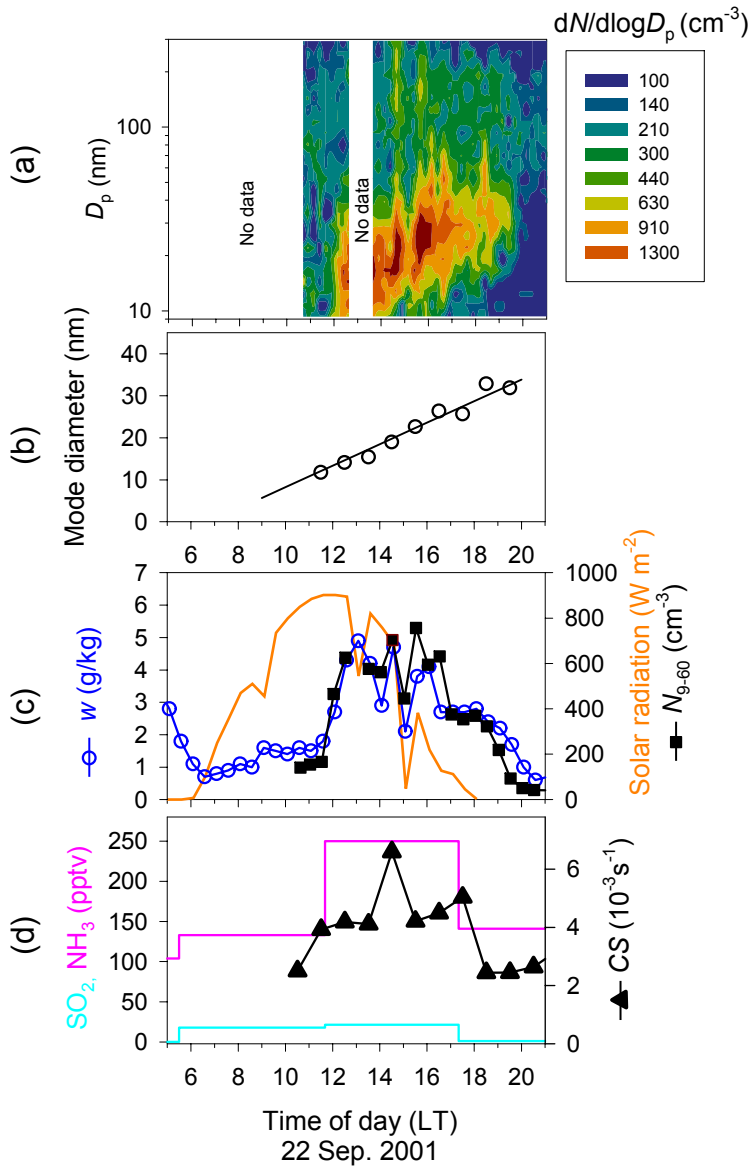

Figure 4-2. Diurnal evolutions of (a) particle number-size distribution in dN/dlogD_p (cm^{-3}), (b) nucleation mode diameter, (c) water vapor mixing rate (w), global solar radiation, and total concentration of particles with 9-60 nm diameters ($N_{9\text{-}60}$), and (d) SO_2 and NH_3 concentrations and CS on 22 September 2001.

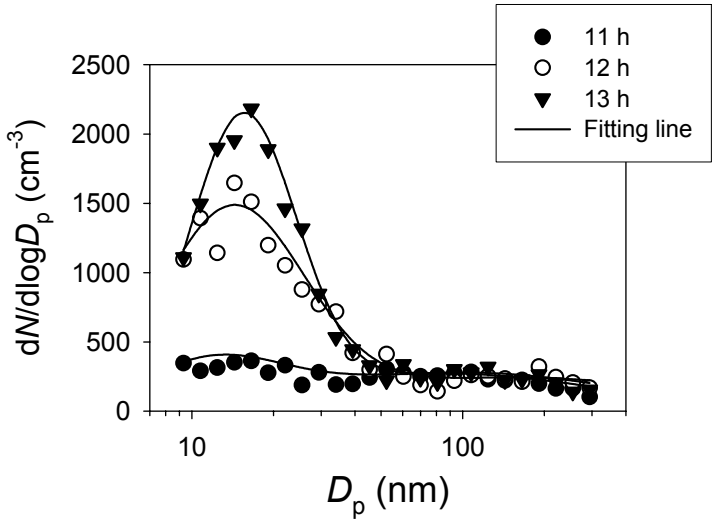

Figure 4-3. Hourly particle size distributions at 11 h, 12 h, and 13 h LT on 22 September 2001. Lines indicate results of log-normal fitting.

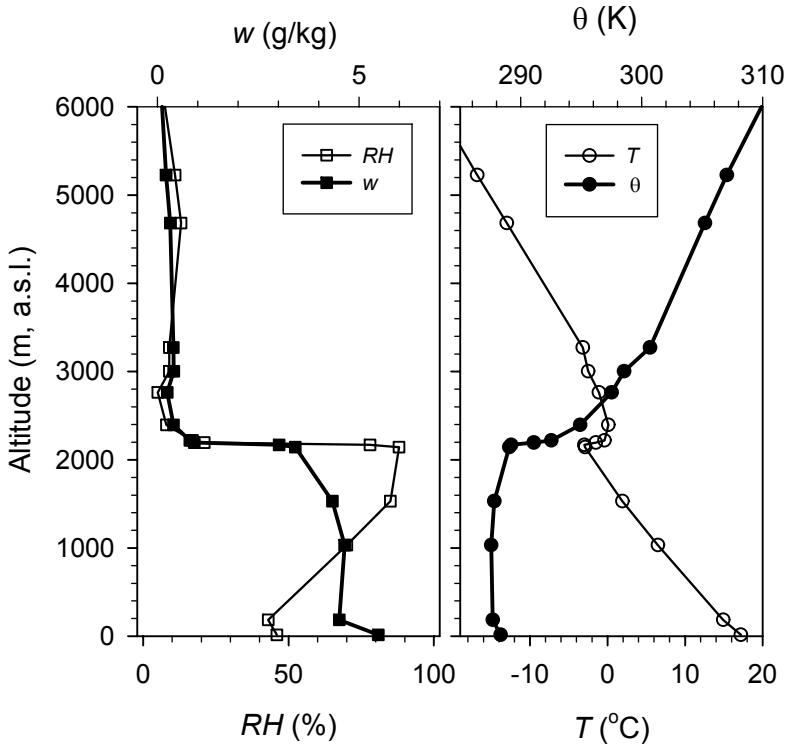

Figure 4-4. Vertical profiles of the relative humidity (*RH*), water vapor mixing rate (*w*), air temperature (*T*), and potential temperature (θ) based on the aerological data at Wajima at 9 h LT of 22 September 2001.

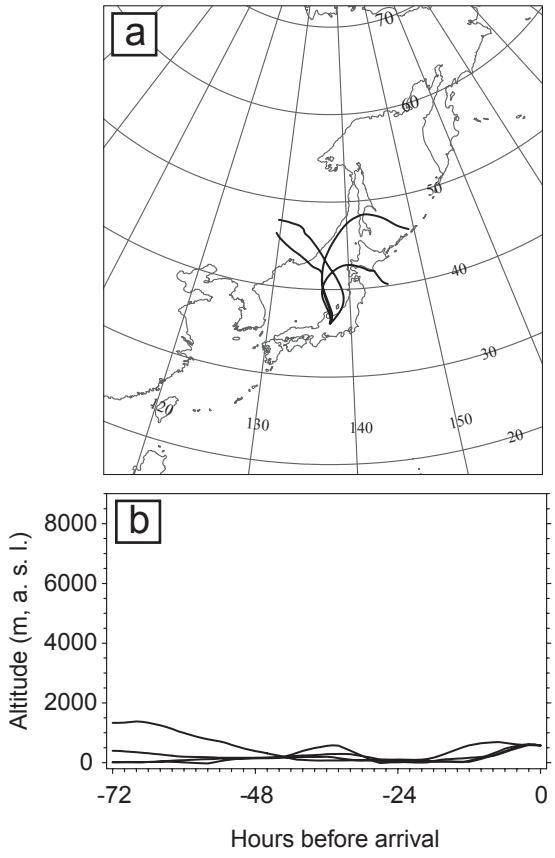

Figure 4-5. (a) Horizontal and (b) vertical backward backtrajectories of air masses from 600 m altitudes near Mt. Norikura at 9 h LT of the NPF event days.

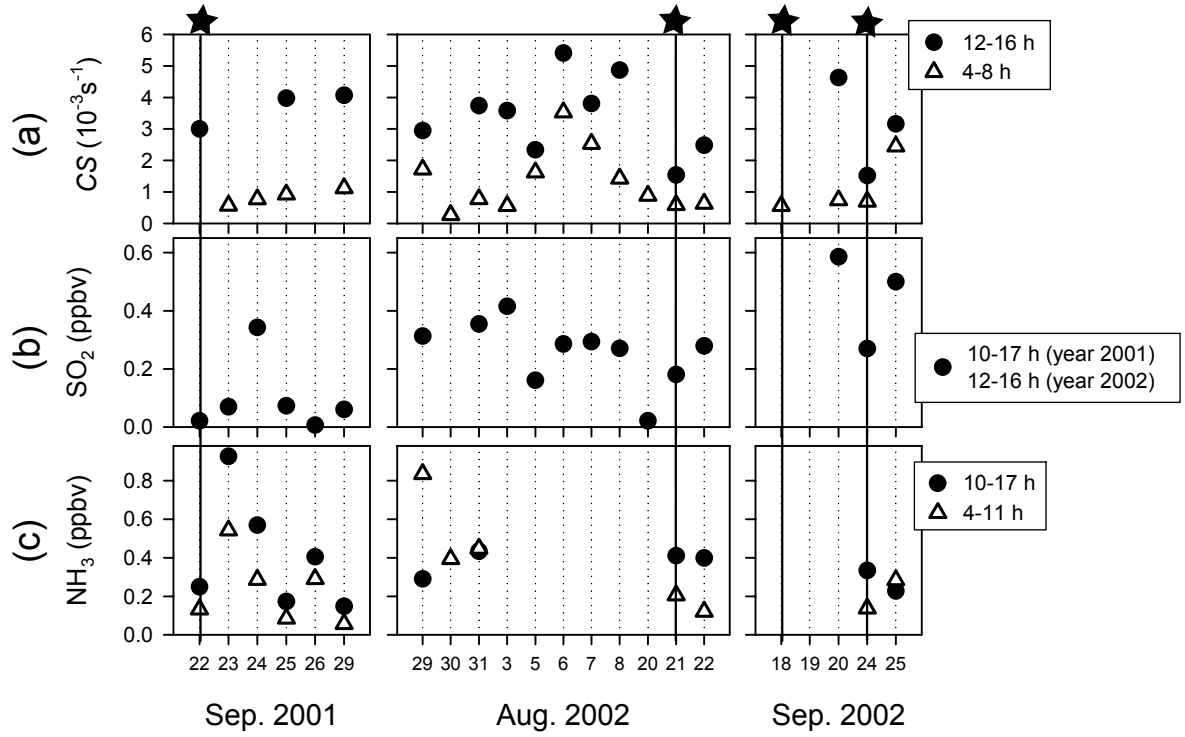

Figure 4-6. Day-to-day variation of (a) *CS*, (b) SO_2 and (c) NH_3 concentrations on sunny days. Black circles and white triangles in Fig. 4-6a respectively denote average *CS* in 4-8 h and 12-16 h LT. Figure 4-5b presents SO_2 concentrations measured by impregnated filter sampling within 10-17 h LT during September 2001 and average SO_2 concentrations in 12-16 h LT during August-September 2002 (mesured using the SO_2 analyzer). Black circles and white triangles in Fig. 4-5c respectively signify NH_3 concentrations measured by impregnated filter sampling within 4-11 h LTand 10-17 h LT. Star marks at the top of Fig. 4-5a indicate the NPF event days.

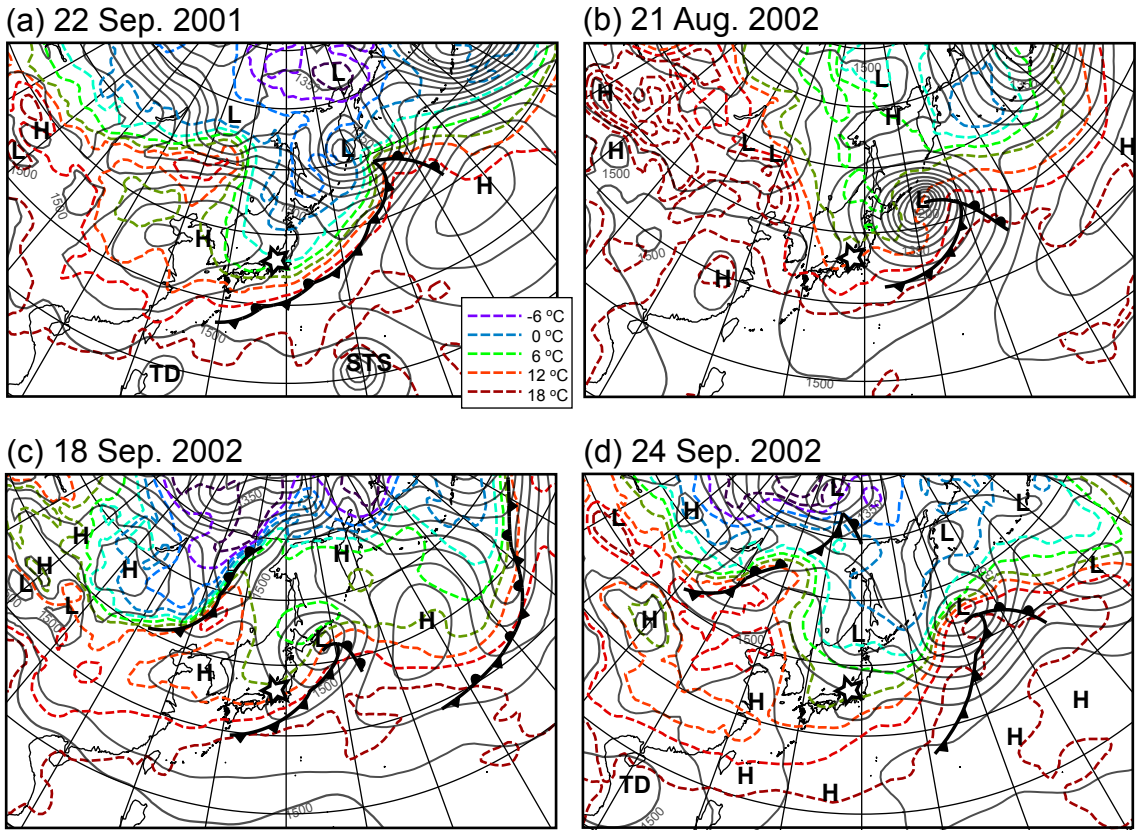

Figure 4-7. Geopotential height (solid lines) and temperature (broken color lines) fields at 850 hPa at 9 h LT of the NPF event days: (a) 22 September 2001, (b) 21 August 2002, (c) 18 September 2002, and (d) 24 September 2002. Location of fronts at the surface level are superimposed on the map. A star mark shows location of the observation site location.

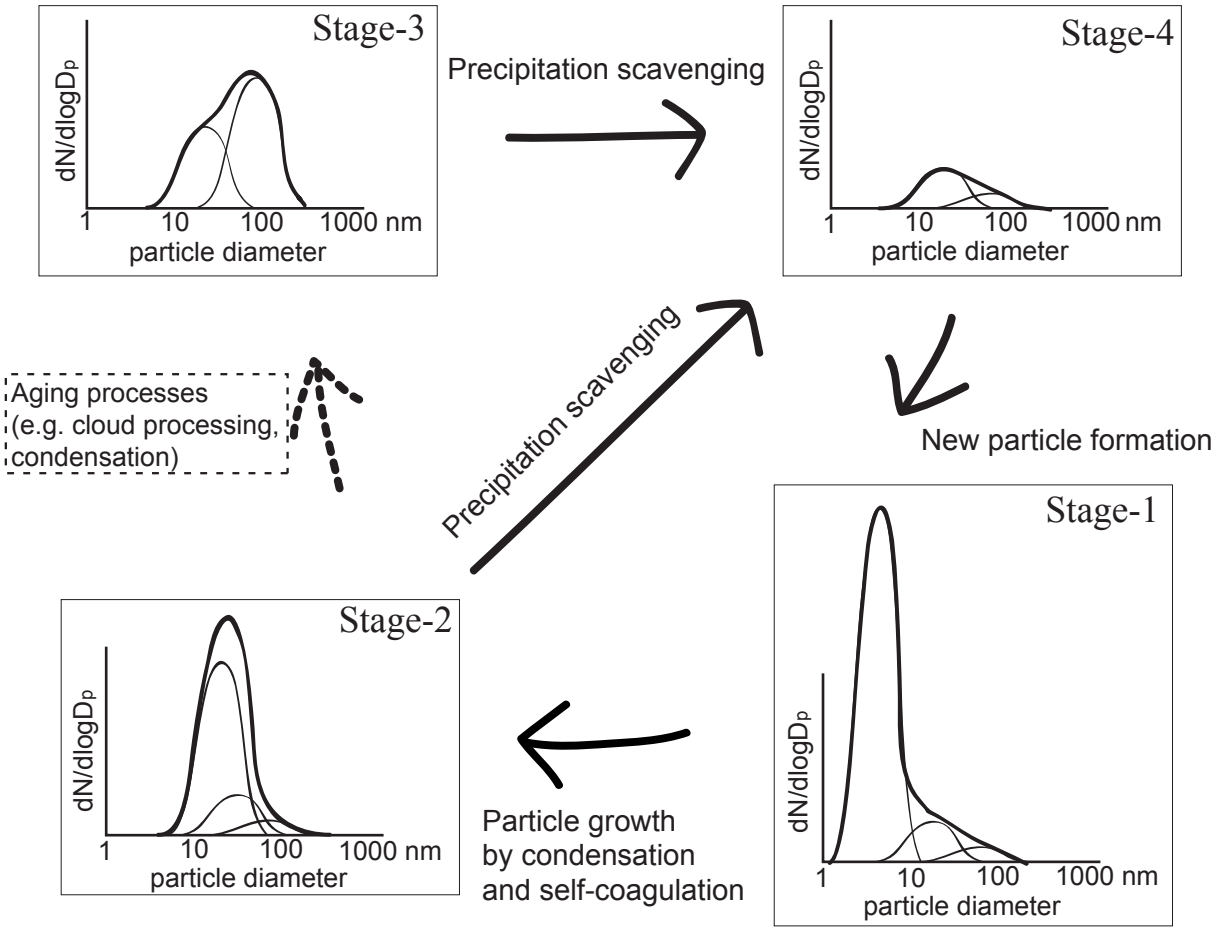

Figure 5-1. Schematic diagram of suggested cycle of number-size distribution of aerosol particles in the atmosphere

副　論　文

1. Number-size distributions of free tropospheric aerosol particles at Mt. Norikura, Japan: Effects of precipitation and air mass transportation pathways,
Nishita C., K. Osada, K. Matsunaga, and Y. Iwasaka,
Journal of Geophysical Research, vol. 112, D10213,
doi:10.1029/2006JD007969,
22 May 2007.

2. Nucleation mode particles in up-slope valley winds at Mt. Norikura, Japan: Implications for the vertical extent of new particle formation events in the lower troposphere,
Nishita C., K. Osada, M. Kido, K. Matsunaga, and Y. Iwasaka,
Journal of Geophysical Research,
Accepted on 17 October 2007.

参 考 論 文

1. Number-size distributions of atmospheric aerosol particles ($10 < D_p < 265$ nm) at Ny-Alesund, Norwegian Arctic: Their relationship with air mass history,
Nishita, C., K Osada, K. Hara, M Kido, M. Wada, T. Shibata, and Y. Iwasaka,
Polar Meteorology and Glaciology, no. 15, 67–77,
November 2001.

2. Temporal variation of water-soluble ions of free tropospheric aerosol particles over central Japan,
Osada, K., M. Kido, C. Nishita, K. Matsunaga, Y. Iwasaka, M. Nagatani, and H. Nakada,
Tellus, 59B, 742–754,
September 2007.

3. Changes in ionic constituents of free tropospheric aerosol particles obtained at Mt. Norikura (2770 m a. s. l.), central Japan, during the Shurin period in 2000,
Osada, K., M. Kido, C. Nishita, K. Matsunaga, Y. Iwasaka, M. Nagatani, and H. Nakada,
Atmospheric Environment , 36, 5469–5477,
24 October 2002.